### Environmental Science Water Research & Technology



### **PERSPECTIVE**

View Article Online



Cite this: DOI: 10.1039/c7ew00159b

# Emerging investigators series: advances and challenges of graphitic carbon nitride as a visible-light-responsive photocatalyst for sustainable water purification†

Qinmin Zheng, D Hongchen Shen D and Danmeng Shuai D\*

Graphitic carbon nitride  $(g-C_3N_4)$  is an emerging visible-light-responsive photocatalyst that has been explored since 2009. This photocatalyst has highly tailorable structures and properties that enable potential utilization of a large portion of solar energy. This material is also synthesized from earth-abundant precursors, is chemically and thermally stable, and is biocompatible with no reported toxicity to date. The merits and pioneering performance evaluation of  $g-C_3N_4$  indicate that this photocatalyst holds promise for the degradation of persistent and emerging contaminants, including chemicals and pathogens, for sustainable water purification with reduced energy and chemical footprint. In this perspective, we propose and answer five questions that are most relevant to the development and application of  $g-C_3N_4$  for photocatalytic water purification, including both benefits and current barriers, from molecular-scale mechanistic understanding of  $g-C_3N_4$  properties and photocatalytic performance to industrial-scale photoreactor design for  $g-C_3N_4$  implementation in practice.

Received 19th May 2017, Accepted 25th July 2017

DOI: 10.1039/c7ew00159b

rsc.li/es-water

### Water impact

Graphitic carbon nitride  $(g\text{-}C_3N_4)$  is an emerging visible-light-responsive photocatalyst, and it is promising for sustainable water purification with reduced energy and chemical consumption. This perspective discusses the benefits and challenges of  $g\text{-}C_3N_4$ -based photocatalysis and provides research insights into the future development and implementation of  $g\text{-}C_3N_4$  for water purification.

A growing number of persistent contaminants are frequently in natural and treated water, pharmaceuticals and personal care products (PPCPs), endocrine disrupting compounds (EDCs), agrochemicals, algal toxins, toxic industrial chemicals, and disinfectant resistant pathogens, and they pose adverse impacts to human health and ecological systems even at very low concentrations (e.g., µgng L<sup>-1</sup>).<sup>1-4</sup> The presence of emerging contaminants further challenges the safety of treated water, such as pollutants hydrofracking, chemical spills (e.g., cyclohexanemethanol spill in Elk River, WV; Deepwater Horizon oil spill in the Gulf of Mexico), and (opportunistic) pathogenic Legionella pneumophila (L. pneumophila), Naegleria fowleri, and Ebola, because the occurrence, toxicity, fate, transport, and transformation of emerging contaminants in natural and engineered systems are underexplored.<sup>5–11</sup> These persistent and emerging contaminants may be recalcitrant to natural degradation and conventional water and wastewater treatment. For example, a recent review suggested that primary and secondary wastewater treatment only achieved 61% removal of PPCPs on average.<sup>12</sup> Advanced treatment technologies, such as membrane filtration (nanofiltration and reverse osmosis) and advanced oxidation processes (AOPs), are shown to enhance the removal of persistent and emerging contaminants; however, they are ill-suited to overcome challenges confronting our sustainable water future due to extensive energy and chemical consumption (*e.g.*, energy and chemical consumption in membrane operation and cleaning; oxidant production, handling, and use for AOPs).<sup>13–15</sup>

Photocatalysis is a promising AOP for the degradation (or even mineralization) of organic contaminants, inactivation of pathogens, and eradication of harmful biofilms. <sup>16–23</sup> Photocatalysis activates dissolved O<sub>2</sub> and/or H<sub>2</sub>O/OH<sup>-</sup> under ambient conditions to generate reactive oxygen species (ROS, *e.g.*, 'OH, O<sub>2</sub>—'/HO<sub>2</sub>', <sup>1</sup>O<sub>2</sub>, H<sub>2</sub>O<sub>2</sub>) and holes (h<sup>+</sup>, also known as electron vacancies) *in situ* to attack contaminants (Scheme 1),

Department of Civil and Environmental Engineering, The George Washington University, Washington, D.C. 20052, USA. E-mail: danmengshuai@gwu.edu; Tel: +1 202 994 0506

† Electronic supplementary information (ESI) available. See DOI: 10.1039/c7ew00159b

and hence it eliminates hurdles in the transport, handling, and storage of oxidants. 16,24-28 ROS and holes are able to oxidize persistent and emerging contaminants effectively due to their high oxidizing power and fast reaction kinetics. Moreover, photocatalysis can use renewable solar energy for water purification, and it promotes sustainable water and wastewater treatment by reducing the energy and chemical demand.

Titanium dioxide (TiO<sub>2</sub>) is the most mature photocatalytic material,  $^{34-37}$  and a broad spectrum of TiO<sub>2</sub>-based photocatalysts have been developed with improved performance for water treatment.  $^{16,23,38}$  However TiO<sub>2</sub> is only reactive under the irradiation of high energy ultraviolet A (UVA) light ( $\lambda$ 



**Qinmin Zheng** 

Qinmin Zheng is a Ph.D. student in the Department of Civil and Environmental Engineering at The George Washington University (GW). His research interest centers on the development of innovative materials for sustainable water treatment, and currently he is working on graphitic carbon nitride-based photocatalytic degradation of persistent organic micropollutants. He is a recipient of a 2017 GW SEAS R&D Showcase Award (Best Ex-

perimental Poster) and a 2017 CAPEES Founding President Best Paper Award. He holds a B.S. degree (2012) in Environmental Chemistry from Jilin University and an M.S. degree (2013) in Environmental Management and Engineering from The Hong Kong Polytechnic University, both in China. < 400 nm) that makes up 4% of the solar spectrum. Visible-light-responsive photocatalysts hold promise for sustainable water purification because they can harvest and potentially utilize more sunlight for reactions (visible light constitutes 40% of solar energy). A broad spectrum of visible-light-responsive photocatalysts have been synthesized and used for lab-scale water treatment studies, such as doped  ${\rm TiO_2}$ , doped tungsten trioxide  ${\rm (WO_3)}$ , silver phosphate  ${\rm (Ag_3PO_4)}$ , bismuth vanadate  ${\rm (BiVO_4)}$ , bismuth oxyhalides  ${\rm (BiOX, X = Cl, Br, and/or I)}$ , metal chalcogenides, and upconversion materials. However, these materials may suffer from low photocatalytic activity, limited photostability, release of toxic chemicals, and potentially high cost for fabrication, and these issues significantly limit their practical engineering application for water purification.

## Introduction of graphitic carbon nitride

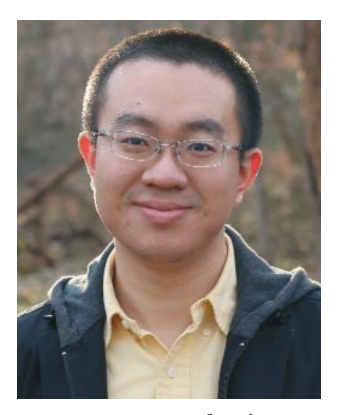
Graphitic carbon nitride (g- $C_3N_4$ ) has emerged as a promising polymeric visible-light-responsive photocatalyst since 2009.  $^{26}$  g- $C_3N_4$  has been considered as the most stable form under ambient conditions compared to its counterpart allotropes (*i.e.*,  $\alpha$ - $C_3N_4$ ,  $\beta$ - $C_3N_4$ , cubic  $C_3N_4$ , pseudocubic  $C_3N_4$ , g-h-triazine, g-otriazine).  $^{47}$  Interestingly, this material is not considered new, because a possible precursor of g- $C_3N_4$ , melon, also known as poly(aminoimino)heptazine, was synthesized back in 1834 by Berzelius and named by Liebig;  $^{48,49}$  however, its catalytic applications were recognized in the past 10 years.  $^{50}$  g- $C_3N_4$  comprises stacked two-dimensional (2D) sheets of heptazine interconnected *via* tertiary amines (Fig. 1);  $^{51}$  but melon is not graphitic – one strand of heptazine units that align in a zigzag manner form hydrogen bonding with an adjacent strand, in contrast to the covalent bond of carbon in graphite, and the strands of



Hongchen Shen

Hongchen Shen is a Ph.D. student in the Department of Civil and Environmental Engineering at The George Washington University (GW). His research interest focuses on the development of visible-light-responsive photocatalysts for antimicrobial applications. He is a recipient of a 2017 GW SEAS R&D Showcase Award (Runner-up) and a 2017 AEESP Stantec Travel Award. He obtained his B.S. and M.S. (2013 and 2016) degrees in Biological

Engineering from Tianjin University, China. His academic background covers biological engineering and environmental science.



**Danmeng Shuai** 

Danmeng Shuai is an assistant professor in the Department of Civil and Environmental Engineering at The George Washington University (GW). He is interaddressing ested in challenges in the water-energyhealth nexus via novel materialbased strategies. His work is currently supported by NSF and USDA-NIFA and has been published in Environ. Sci. Technol., ACS Catal., ACS Appl. Mater. Interfaces, ACS Sustainable Chem.

Eng. etc. He obtained his Ph.D. degree from the University of Illinois at Urbana-Champaign (2012) and his M.E. and B.E. degrees from Tsinghua University (2007 and 2005), all in Environmental Engineering. He worked as a postdoctoral researcher at the University of Iowa (2012–2013).

### Charge Separation Pathway for ROS production

Photocatalyst +  $hv \to e^-$  (conduction band) +  $h^+$  (valence band)  $O_2 + e^- \to O_2^- \cdot E_0' = -0.33 V$   $HO_2 \to O_2^- \cdot + H^+ pK_a = 4.8$   $O_2^- \cdot + 2H^+ + e^- \to H_2O_2 E_0' = 0.89 V$   $H_2O_2 \to HO_2^- + H^+ pK_a = 11.7$   $O_2 + 2H^+ + 2e^- \to H_2O_2 E_0' = 0.28 V$   $H_2O_2 + e^- \to 0H^- + \cdot 0H E_0' = 0.38 V$   $H_2O_1 + e^- \to 0H^- + \cdot 0H + H^+ E_0' = 2.32 V$   $\cdot 0H \to 0^- \cdot + H^+ pK_a = 11.8$   $2HO_2 \to {}^{-1}O_2 + H_2O_2$  $O_2^- \cdot + h^+ \to {}^{-1}O_2 E_0' = 0.65 V$ 

#### Interactions Between Radicals

$$2HO_{2} \to H_{2}O_{2} + O_{2}$$

$$HO_{2} \cdot +O_{2}^{-} \cdot +H_{2}O \to H_{2}O_{2} + O_{2} + OH^{-}$$

$$2 \cdot OH \to H_{2}O_{2}$$

$$H_{2}O_{2} + hv (UV) \to 2 \cdot OH$$

$$H_{2}O_{2} + O_{2}^{-} \to OH + O_{2} + OH^{-}$$

#### Energy Transfer Pathway for ROS production

$${}^{3}O_{2} + hv \xrightarrow{Intersystem\ Crossing} {}^{1}O_{2}$$

### Overall Photocatalytic Oxidation

$$ROS, h^+ + contaminants \rightarrow oxidized \ products \ (e.\ g.\ , H_2O, CO_2)$$

$$O_2 + contaminants + hv \xrightarrow{Photocatalyst} oxidized \ products \ (e. g., H_2O, CO_2)$$

Scheme 1 Photocatalytic oxidation for contaminant transformation. Photocatalytic oxidation for contaminant transformation. Reduction potentials  $E'_0$  are determined under the following conditions: 1 bar or 1 atm of  $O_2$ , 1 M of  $O_2$ ,  $O_2$ , and  $O_2$ , and  $O_3$ , and  $O_4$ , are also as a substitute of  $O_4$ , and  $O_4$ , and  $O_4$ , are also as a substitute of  $O_4$ , and  $O_4$ , are also as a substitute o

heptazine units stack up  $via \pi^{-\pi}$  interactions (Fig. 1). Melon is more thermodynamically stable than g-C<sub>3</sub>N<sub>4</sub> under typical experimental conditions (*e.g.*, in thermal polycondensation); <sup>52,53</sup> however, melon was always recognized as g-C<sub>3</sub>N<sub>4</sub> in the current scientific literature, due to its X-ray powder diffraction pattern with a pseudo-graphitic peak. <sup>54</sup> The readers should be aware that melon is most likely to be present in most studies, though we will still use the term g-C<sub>3</sub>N<sub>4</sub> for melon in this perspective.

g-C<sub>3</sub>N<sub>4</sub> has been reported for a broad range of photocatalytic applications to date, including H<sub>2</sub> evolution from water splitting, CO<sub>2</sub> reduction, selective oxidation for organic synthesis, germicides, and environmental remediation.<sup>55–62</sup> Direct water splitting for H<sub>2</sub> production and converting CO<sub>2</sub> into CO or hydrocarbons by photocatalysis is an ideal strategy for large scale

utilization and conversion of inexhaustible solar energy. g- $C_3N_4$ -based photocatalysis holds promise for artificial photosynthesis and renewable energy related applications, because the photocatalyst can harvest and utilize more solar energy in the visible range, has suitable band energy levels for water and  $CO_2$  reduction, and exhibits high photocatalytic activity (apparent quantum yield up to 16.7% and 5.7% for  $H_2$  evolution and  $CO_2$  reduction, respectively).<sup>55</sup> In addition to acting as a photocatalyst, g- $C_3N_4$  has diverse applications for catalysis, <sup>49,63</sup> selective membrane separation, <sup>64</sup> sensing, <sup>65,66</sup> bioimaging, <sup>67</sup> optoelectronics, <sup>68</sup> and electrochemical devices, <sup>54</sup> because of the unique properties of this material. <sup>69</sup>

The past few years have witnessed a surge of interest in the area of g-C<sub>3</sub>N<sub>4</sub>-based photocatalysis. A quick search

Fig. 1 The structures of (a) melon and (b)  $g-C_3N_4$ . Reproduced from ref. 54 and 55 with permission from the Nature Publishing Group and the American Chemical Society.

using the terms 'photocatal\*', 'g-C<sub>3</sub>N<sub>4</sub>' or 'graphitic carbon nitride', and 'contaminant' or 'pollutant' as topic keywords in the ISI Web of Science database indicated a rising interest in using g-C<sub>3</sub>N<sub>4</sub> as a photocatalyst for environmental remediation (Fig. 2). Several comprehensive reviews have systematically summarized the synthesis, properties, and engineering applications of photocatalytic g-C3N4, and a focus on environmental some of them have remediation. 29,49,51,54,55,70-76 Readers are encouraged to read these reviews to understand the state-of-the-art discoveries of g-C<sub>3</sub>N<sub>4</sub>. We summarized the representative photocatalytic activity of g-C<sub>3</sub>N<sub>4</sub>-based photocatalysts for degrading/ inactivating waterborne contaminants, including phenolic compounds, antibiotics, agrichemicals, pharmaceuticals, and microorganisms, in Table S1† (2011-2017). In contrast to the reviews, our perspective will center on the opportunities and challenges of developing g-C3N4 for water and wastewater treatment. In our understanding, a gigantic

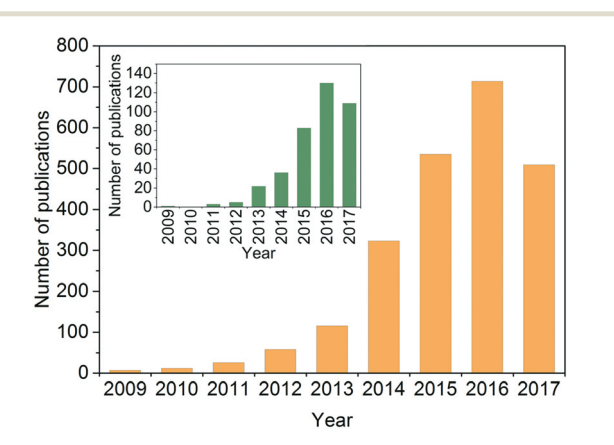


Fig. 2 The number of annual journal publications using the combined 'photocatal\*' and 'graphitic carbon nitride' or 'g- $C_3N_4$ ' as subjects since 2009, and (inset) the refined result by including the subject 'contaminant' or 'pollutant'. Adapted from the ISI Web of Science, dated Jun 10, 2017.

number of g- $C_3N_4$  samples have been synthesized since 2009; however, the key properties determining photocatalytic performance have not been identified, the degradation of persistent and emerging contaminants (rather than synthetic dyes) in real, complex water matrices is largely unknown, and a universally accepted standard for testing and comparing the photocatalytic performance of different g- $C_3N_4$  samples has not been developed. Our perspective proposes five critical questions related to the development and application of g- $C_3N_4$  for water purification that the readers will be most interested in (Fig. 3). This perspective aims to shed light on current research needs in this area and guide future design and engineering applications of the photocatalyst in practice.

# Question 1: what are the benefits and potential pitfalls of using g-C<sub>3</sub>N<sub>4</sub> as a visible-light-responsive photocatalyst for water purification?

g- $C_3N_4$  samples are commonly synthesized from N-rich organic precursors (*e.g.*, urea, melamine, cyanamide, dicyandiamide, thiourea) via thermal polycondensation, solvothermal methods, and electrochemical methods.<sup>70</sup> The backbone of g- $C_3N_4$  only contains earth-abundant elements of carbon and nitrogen that enable inexpensive, large-scale material

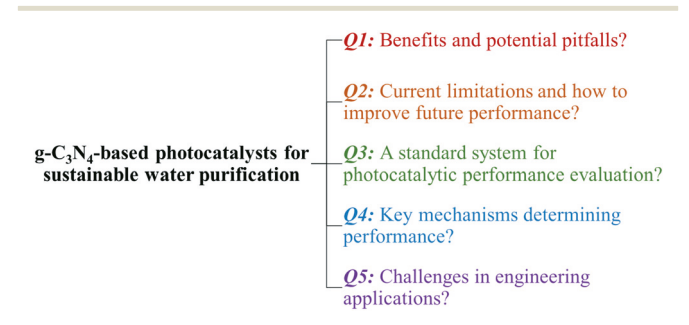


Fig. 3 Five questions about  $g-C_3N_4$ -based photocatalysts for sustainable water purification that are addressed in our perspective.

fabrication. g-C<sub>3</sub>N<sub>4</sub> can also be potentially synthesized from renewable or waste materials (e.g., urea from urine). Bulk g-C<sub>3</sub>N<sub>4</sub>, e.g., the one synthesized from melamine-only, is responsive to ultraviolet (UV) and visible light up to 460 nm, due to its band gap of 2.7 eV.<sup>77</sup> This band gap originates mainly from nitrogen and carbon p<sub>2</sub> orbitals, which contribute to the formation of valence and conduction bands, respectively.26,78 A range of g-C<sub>3</sub>N<sub>4</sub> samples have been reported, e.g., mesoporous g-C<sub>3</sub>N<sub>4</sub>,<sup>79</sup> doped g- $C_3N_4$ ,<sup>79-83</sup> solvothermal g- $C_3N_4$ ,<sup>84</sup> guanazole derived g- $C_3N_4$ ,<sup>85</sup> acid or base treated g- $C_3N_4$ ,<sup>86,87</sup> and g- $C_3N_4$  nanosheets, 80 with a tunable band gap of 1.5-2.9 eV that are able to harvest UV-visible or even near-infrared light up to 827 nm. 84,85,87 Dopants with different electronegativity compared to C or N induce band gap variations,88 and a strong quantum confinement effect for g-C<sub>3</sub>N<sub>4</sub> nanosheets and a reduced electron density of protonated g-C<sub>3</sub>N<sub>4</sub> result in an increased band gap. 89,90 Solvothermal g-C<sub>3</sub>N<sub>4</sub> or guanazole derived g-C<sub>3</sub>N<sub>4</sub> was prepared from a distinct precursor (e.g., cyanuric chloride, guanazole) or through a different reaction pathway (e.g., a solvothermal reaction) compared to thermal polycondensation, and the material may have a unique structure and a resulting band gap. 70,84,85 The broad band gap indicates that g-C<sub>3</sub>N<sub>4</sub> can potentially utilize up to 8-62% of solar energy (calculated based on solar spectral irradiance, AM 1.5, terrestrial global 37° south facing tilt), in contrast to the widely studied TiO<sub>2</sub> that can only use 4% of the solar energy. The application of g-C<sub>3</sub>N<sub>4</sub> for water purification can potentially boost the reactivity for contaminant degradation and pathogen inactivation with significantly reduced energy and chemical footprint, which promotes sustainable water and wastewater treatment.

Moreover, g-C<sub>3</sub>N<sub>4</sub> is thermally and chemically stable (e.g., resistant to air oxidation up to 600 °C; insoluble in water, organic solvents, bases, and diluted acids), exhibits no reported toxicity to date, and its properties and performance are highly tunable for enhanced performance due to the polymeric nature of this material. 91-93 All these merits enable g-C<sub>3</sub>N<sub>4</sub> to be an ideal photocatalyst for sustainable water purification.

One dilemma that photocatalysis is facing is how to appropriately tailor the band gap of a photocatalyst. Reduction of the band gap enables harvesting photons with a lower energy or a longer wavelength, which promotes the utilization of more solar energy. However, harvesting lower energy photons does not necessarily translate into improved photocatalytic performance, because photogenerated charges (i.e., electrons and holes) with a reduced energy level, or reduced oxidizing or reduction power, cannot activate O2/H2O, oxidize contaminants, and/or inactivate pathogens effectively. For example, a g-C<sub>3</sub>N<sub>4</sub> sample with the lowest reported band gap of 1.5 eV showed an 8.4-fold decrease of reactivity for Rhodamine B degradation in contrast to another g-C<sub>3</sub>N<sub>4</sub> sample with a band gap of 2.1 eV, though both samples were synthesized from triazole precursors. 85 Fig. 4 summarizes a number of g-C<sub>3</sub>N<sub>4</sub> samples and reference photocatalysts with their reported band gaps and band energy levels, in comparison with the reduction potentials  $E'_0$  of ROS. Fig. 4 clearly shows that some g-C<sub>3</sub>N<sub>4</sub> samples with a reduced band gap cannot produce ROS (i.e., O2-',HO2') or oxidize contaminants under thermodynamically favorable conditions. These samples may be responsive to low energy photons and generate separated charges, but the charges tend to recombine rather than promote contaminant degradation and pathogen inactivation.

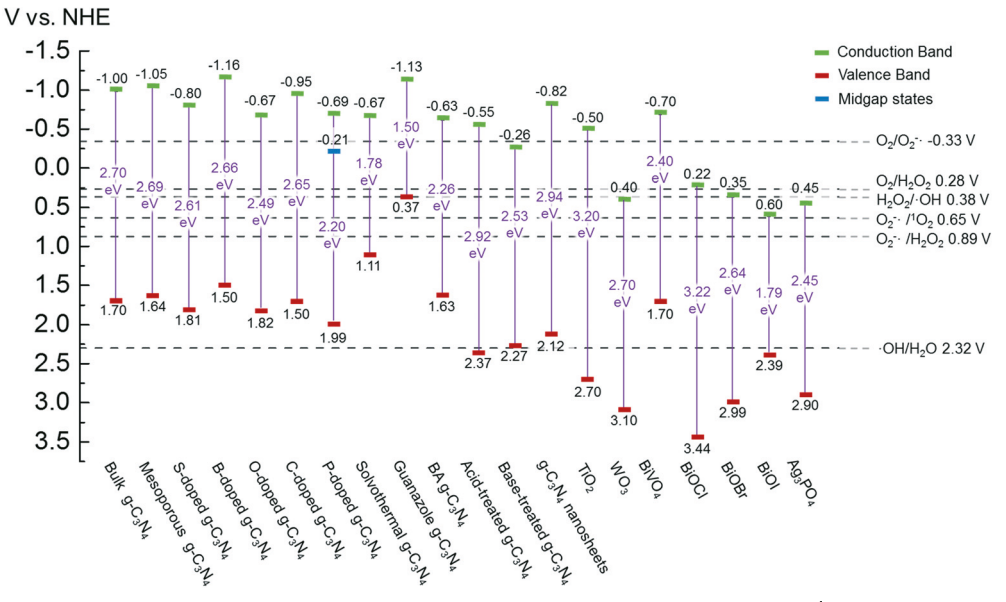


Fig. 4 Band structures of typical g-C<sub>3</sub>N<sub>4</sub> samples and reference photocatalysts, and reduction potentials  $E_0'$  of ROS generation. <sup>55</sup> g-C<sub>3</sub>N<sub>4</sub> samples include bulk g-C<sub>3</sub>N<sub>4</sub> (undoped), <sup>79</sup> mesoporous g-C<sub>3</sub>N<sub>4</sub>, <sup>79</sup> S-doped g-C<sub>3</sub>N<sub>4</sub>, <sup>80</sup> O-doped g-C<sub>3</sub>N<sub>4</sub>, <sup>82</sup> C-doped g-C<sub>3</sub>N<sub>4</sub>, <sup>81</sup> P-doped g-C<sub>3</sub>N<sub>4</sub>, <sup>80</sup> solvothermal g-C<sub>3</sub>N<sub>4</sub>, <sup>84</sup> guanazole g-C<sub>3</sub>N<sub>4</sub>, <sup>85</sup> BA g-C<sub>3</sub>N<sub>4</sub> (synthesized from barbituric acid (BA)), <sup>94</sup> acid-treated g-C<sub>3</sub>N<sub>4</sub> (protonated), <sup>87</sup> base-treated g-C<sub>3</sub>N<sub>4</sub>, <sup>86</sup> g-C<sub>3</sub>N<sub>4</sub> nanosheets, <sup>80</sup> TiO<sub>2</sub>, <sup>95</sup> WO<sub>3</sub>, <sup>96</sup> BiVO<sub>4</sub>, <sup>97</sup> BiOX (X = Cl, Br, and/or I), <sup>42</sup> and Ag<sub>3</sub>PO<sub>4</sub>, <sup>98</sup> NHE represents normal hydrogen electrode. Reduction potentials  $E'_0$  are determined under the following conditions: 1 bar or 1 atm of  $O_2$ , 1 M of  $O_2^-$ ,  $H_2O_2$ , and  $O_1$ ,  $O_2$ ,  $O_3$ ,  $O_4$ ,  $O_$ 25 °C.

The chemical stability of g-C<sub>3</sub>N<sub>4</sub> should also be evaluated for long-term photocatalytic water purification. Unlike many stable inorganic photocatalysts (e.g., TiO2, ZnO) that are not susceptible to photocorrosion, g-C<sub>3</sub>N<sub>4</sub> is a polymer and could be decomposed into organic carbon, organic nitrogen, CO, CO<sub>2</sub>, NO<sub>x</sub>, NO<sub>2</sub>, and/or NO<sub>3</sub> in photocatalytic oxidation. Holes and electrons are produced in the photoreaction; however, the holes are much less mobile than the electrons (i.e., diffusion length of several nanometers vs. micrometers), 99 and the holes could oxidize the g-C<sub>3</sub>N<sub>4</sub> matrix prior to its migration to the photocatalyst surface and reaction with contaminants/pathogens. One study explored the photoreduction of isotope-labeled <sup>13</sup>CO<sub>2</sub> on g-C<sub>3</sub>N<sub>4</sub>, and it provided solid experimental proof that the product <sup>13</sup>CO came from <sup>13</sup>CO<sub>2</sub>. <sup>100</sup> No <sup>12</sup>CO was detected, which may suggest that g-C<sub>3</sub>N<sub>4</sub> was photostable in the reaction (g-C<sub>3</sub>N<sub>4</sub> was not isotopically labeled with <sup>13</sup>C). To the best of our knowledge, only one reference reported the photostability of g-C<sub>3</sub>N<sub>4</sub> in a 5 h NO oxidation experiment (W-type fluorescent lamp, 6000 lx,  $\lambda > 380$  nm), and 9 wt% of g-C<sub>3</sub>N<sub>4</sub> was expected to be decomposed under continuous photocatalytic oxidation for 1 year. 101 However, the NO oxidation experiment was only conducted for a short duration, the observed g-C<sub>3</sub>N<sub>4</sub> selfdegradation in a gas phase reaction may not be representative of aqueous phase reactions in water purification, g-C<sub>3</sub>N<sub>4</sub> with distinct properties (e.g., porosity, surface area, dopants, surface functional groups) may show various photostability, and contaminant/pathogen properties and complex water matrices may significantly impact g-C<sub>3</sub>N<sub>4</sub> self-degradation. For instance, g-C<sub>3</sub>N<sub>4</sub> with an enlarged surface area could promote hole migration to the material surface, and a contaminant that shows a strong interaction with g-C<sub>3</sub>N<sub>4</sub> could scavenge the holes readily. The photocorrosion of g-C<sub>3</sub>N<sub>4</sub> could be inhibited under both scenarios. To systematically evaluate photocorrosion, total organic carbon and nitrogen should be measured in photocatalytic reactions. More specifically, g-C<sub>3</sub>N<sub>4</sub> could be isotopically labeled with <sup>13</sup>C or <sup>15</sup>N in synthesis, and it will facilitate identifying the origin of reaction products. It is critical to understand the photostability of g-C<sub>3</sub>N<sub>4</sub> before its engineering implementation for the treatment of real water and wastewater.

The potential adverse impacts of g-C<sub>3</sub>N<sub>4</sub> to humans and ecological systems are also largely underexplored. Many metal and non-metal nitrides (e.g., BN, Si<sub>3</sub>N<sub>4</sub>, TiN) have been approved by the U.S. Food and Drug Administration (FDA) for use in food contact surfaces, 102 which suggests that the emerging photocatalyst g-C<sub>3</sub>N<sub>4</sub> could also exhibit little to no toxicity. One study reported that g-C<sub>3</sub>N<sub>4</sub> in the form of nanosheets showed great biocompatibility because it did not inhibit the growth of murine fibroblasts.<sup>91</sup> Our preliminary study also supports this argument: g-C<sub>3</sub>N<sub>4</sub> did not inhibit the growth of Escherichia coli (E. coli) and Staphylococcus epidermidis in the dark, though the photocatalyst inactivated both microorganisms effectively under visible light irradiation due to ROS production and their attack on the bacteria (data not shown). However, systematic toxicity evaluation of g-C<sub>3</sub>N<sub>4</sub>, especially in the form of nanoparticles, nanorods, and nanosheets, should be conducted in microorganisms, plant cells, and/or mammal cells to understand the potential risks of g-C<sub>3</sub>N<sub>4</sub> to humans and ecological systems in engineering applications. In addition, the toxicity of selfdecomposed g-C<sub>3</sub>N<sub>4</sub> and its daughter products in photocatalytic reaction should also be considered, because self-decomposition could release toxic, soluble organic fragments from g-C<sub>3</sub>N<sub>4</sub>.

Scalable production of g-C<sub>3</sub>N<sub>4</sub> is also of great interest for its engineering application. The current yield of g-C<sub>3</sub>N<sub>4</sub> in thermal polycondensation is 5-30 wt% based on our previous studies, depending on precursor selection, and the fabrication of g-C<sub>3</sub>N<sub>4</sub> nanosheets with improved photocatalytic performance has a much lower yield (4-6 wt% yield compared to the precursor). Yuan et al. reported, for the first time, that a g-C<sub>3</sub>N<sub>4</sub> sample with a high yield (~61 wt%) was prepared by heating melamine in a vacuum-sealed environment (3-10 mbar). However, the g-C<sub>3</sub>N<sub>4</sub> yield prepared by solvothermal or electrochemical methods is unknown, and how to improve the yield in different synthetic methods is underexplored. In addition, the economic cost, energy consumption, and environmental impacts should be evaluated for material fabrication, e.g., by life cycle assessment, prior to the application for water purification.

### Question 2: what factors are the major hurdles limiting the photocatalytic performance of g-C<sub>3</sub>N<sub>4</sub> for water purification and how can its performance be improved?

Increasing the surface area, charge separation, solar energy utilization, and ROS production of g-C<sub>3</sub>N<sub>4</sub> are believed to increase the photocatalytic activity of a material and enable its industrial-scale water purification in the future. The improved surface area of a photocatalyst usually promotes its reactivity, because the material provides more reaction sites and reduces the recombination of photogenerated electrons and holes. The holes are much less mobile than the electrons,99 and the increased surface area could facilitate hole migration to the surface and subsequent reactions, rather than hole recombination with electrons and consequent energy dissipation. g-C<sub>3</sub>N<sub>4</sub> synthesized from the thermal polycondensation of melamine or dicyandiamide, a typical N-rich precursor, generally shows a limited surface area  $(<10 \text{ m}^2 \text{ g}^{-1})$  (Fig. 5a). Urea-based g-C<sub>3</sub>N<sub>4</sub> exhibits an increased surface area, as well as photocatalytic activity, likely due to a large amount of gaseous by-product emission (e.g., NH<sub>3</sub>, H<sub>2</sub>O) in thermal polycondensation. Several strategies have taken advantage of the gaseous by-product formation by introducing a precursor with low thermal stability to create pores and improve the surface area. For example, NH<sub>4</sub>Cl was blended with dicyandiamide for g-C<sub>3</sub>N<sub>4</sub> synthesis, and the precursors yielded g-C<sub>3</sub>N<sub>4</sub> nanosheets with a significantly increased surface area (52.9 vs. 2.9 m<sup>2</sup> g<sup>-1</sup>) (Fig. 5b).<sup>104</sup> A more sophisticated supramolecular approach, also known as soft templating, was introduced to increase the surface area of g-C<sub>3</sub>N<sub>4</sub>. Briefly, the precursors form a supramolecular complex via hydrogen bonding (e.g., melamine and cyanuric acid), and they produce porous g-C3N4 after thermal polycondensation because one precursor (e.g., cyanuric acid) is thermally unstable and decomposes into gaseous by-products.

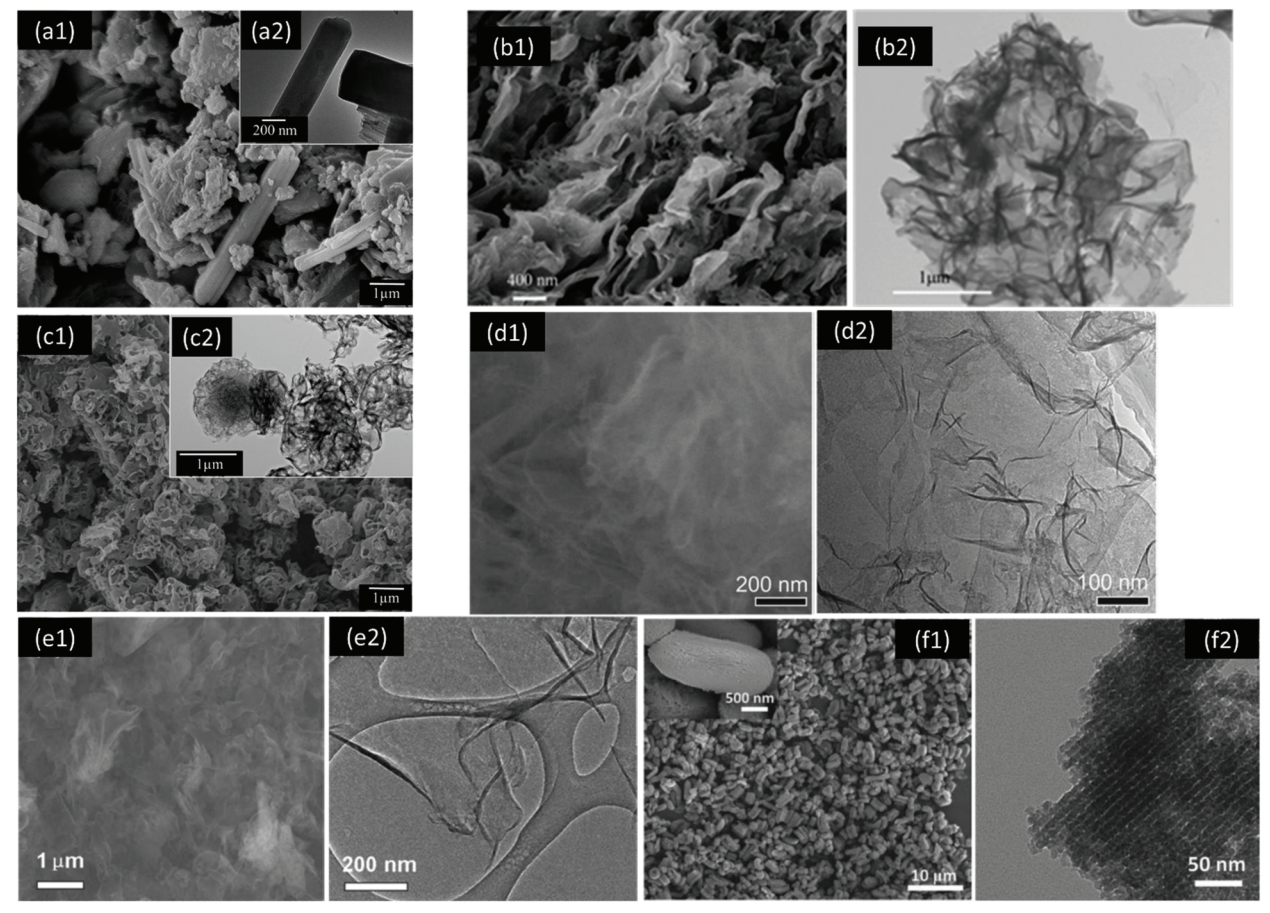


Fig. 5 Scanning electron microscopy (SEM) and transmission electron microscopy (TEM) of (a1 and a2) g-C<sub>3</sub>N<sub>4</sub> synthesized from melamine,<sup>77</sup> (b1 and b2) g-C<sub>3</sub>N<sub>4</sub> nanosheets synthesized from dicyandiamide and NH<sub>4</sub>Cl,<sup>104</sup> (c1 and c2) porous g-C<sub>3</sub>N<sub>4</sub> synthesized from melamine and cyanuric acid via a supramolecular method,<sup>77</sup> (d1 and d2) g-C<sub>3</sub>N<sub>4</sub> nanosheets synthesized via thermal exfoliation,<sup>90</sup> (e1 and e2) g-C<sub>3</sub>N<sub>4</sub> nanosheets synthesized via liquid exfoliation, <sup>106</sup> and (f1 and f2) mesoporous g-C<sub>3</sub>N<sub>4</sub> synthesized using silica as a hard template. <sup>107</sup> Reproduced from ref. 77, 90, 104, 106 and 107 with permission from the American Chemical Society, the Royal Society of Chemistry, and Wiley-VCH.

Our previous study indicated that the surface area was significantly enhanced 8.0-fold, from 9.8 m<sup>2</sup> g<sup>-1</sup> (melamine-based g-C<sub>3</sub>N<sub>4</sub>) to 78.8 m<sup>2</sup> g<sup>-1</sup> (melamine-cyanuric acid-based g-C<sub>3</sub>N<sub>4</sub>) (Fig. 5c).<sup>77</sup> Thermal exfoliation and liquid exfoliation are two most widely studied approaches that have been used to produce g-C<sub>3</sub>N<sub>4</sub> nanosheets with a much higher surface area to improve the photocatalytic activity. 105 Briefly, assynthesized bulk g-C<sub>3</sub>N<sub>4</sub> is subjected to post-thermal treatment in air (e.g., 500 °C) or ultrasonication in a solvent with a favorable surface energy (e.g., water, isopropanol) to produce g-C<sub>3</sub>N<sub>4</sub> nanosheets. The surface area of the nanosheets was as high as 306 or 384 m<sup>2</sup> g<sup>-1</sup> after thermal exfoliation (Fig. 5d) or liquid exfoliation (Fig. 5e), respectively. 90,106 The hard templating approach, which is almost identical with the conventional casting process, utilizes hard templates that are resistant to thermal treatment (e.g., silica nanoparticles, ordered mesoporous silica, anodic aluminum oxide, and calcium carbonate) to design a range of structures and geometries of g-C<sub>3</sub>N<sub>4</sub> and to construct hierarchical pore architectures.55 Well-defined pore sizes and distribution of g-C<sub>3</sub>N<sub>4</sub> were achieved via this approach, as well as a significantly improved surface area (517 m<sup>2</sup> g<sup>-1</sup>) (Fig. 5f). <sup>107</sup> However, post-treatment of removing the hard templates via corrosive, toxic chemicals (e.g., HF, NH<sub>4</sub>HF<sub>2</sub>) to create pores may limit large-scale, sustainable material fabrication of g-C<sub>3</sub>N<sub>4</sub>.

Improving charge separation promotes more photogenerated electrons and holes for reactions. In addition to increasing the surface area of g-C<sub>3</sub>N<sub>4</sub> by creating a porous structure or fabricating nanoscale materials, functionalization of a photocatalyst also leads to promoted charge separation. Elemental doping of non-metals (e.g., O, C, N, P, S, B, and halogens) and metals (e.g., Fe, Zn, Cu, and Ni), as well as molecular doping (e.g., electrondonating or electron-withdrawing organic molecules), has been shown to promote the delocalization of  $\pi$  electrons in the g-C<sub>3</sub>N<sub>4</sub> structure and thus improve charge separation. 29,49,51,55,70,71 The introduction of defects (e.g., nitrogen or carbon vacancies)108-111 or structural distortion112,113 via postthermal treatment in hydrogen, ammonia, or argon gas of synthesized g-C<sub>3</sub>N<sub>4</sub> also exhibits improved charge separation. Steady-state and time-resolved photoluminescence (PL), photocurrent analyses, and density functional theory (DFT) calculations have been used as experimental and simulation tools to

demonstrate the improved charged separation of tailored g-C<sub>3</sub>N<sub>4</sub> structures. The steady-state PL quantum yield (QY) was 4.8%, 5.5-19.6%, and 14.5-96% for bulk, nanosheet, and nanoparticulate (quantum dot, QD) g-C3N4, respectively (Table S2†). 65,114-120 Time-resolved PL measurements are believed to be more informative than steady-state PL analyses, because fluorescence lifetimes are typically independent of the probe concentration during analysis. 121,122 The average fluorescence lifetime (AFL) of representative photocatalysts in time-resolved PL measurements are summarized in Table S3,† and the AFL of g-C<sub>3</sub>N<sub>4</sub> was comparable to those of other widely studied photocatalysts for water purification (i.e., TiO2, WO3, BiVO4). Bulk g-C3N4 showed a wide range of AFL (2.42-9.86 ns), depending on the precursor (e.g., dicyandiamide, melamine, urea) and measureconditions emission (e.g., excitation and wavelengths). 80,87,90,123-128 Modifications of g-C<sub>3</sub>N<sub>4</sub>, e.g. P-doping, protonation, the creation of an open structure, and exfoliation into nanosheets, increased the AFL to 3.927-18.4 ns, which could be related to improved charge localization in the g-C<sub>3</sub>N<sub>4</sub> matrix. 80,87,90,125,127 In general, a long AFL in photoluminescence improves the likelihood of a photocatalytic event occurring, 129 and the tailored g-C<sub>3</sub>N<sub>4</sub> samples exhibited enhanced photocatalytic activity. In contrast, the introduction of barbituric acid, quinoline, nitrogen defects (via hydrogenation), and dopant K and/or OH into the g-C<sub>3</sub>N<sub>4</sub> structure decreased the AFL to 0.58– $3.3~{\rm ns}^{124,126,128,129}$  but the photocatalytic activity of these samples was still enhanced. The decrease of AFL suggests a new deactivation mechanism involving nonradiative recombination, presumably by transferring charges to new localized states (e.g., the formation of heterojunctions). 123 PL provides evidence of the extent and rate of radiative recombination in photocatalysis; however, many other factors could influence the photocatalytic performance simultaneously.

Functionalization and post-thermal treatment of assynthesized g-C<sub>3</sub>N<sub>4</sub> in a controlled atmosphere were also observed to improve the visible light response by harvesting more photons of a longer wavelength.<sup>55</sup> In addition, g-C<sub>3</sub>N<sub>4</sub> synthesized via a solvothermal method using cyanuric chloride with melamine or cyanuric acid in acetonitrile resulted in a reduced band gap of 1.8-2.3 eV (responsive to  $\lambda < 539$ -689 nm).84,130 The band gap reduction could have resulted from a unique chlorine doped g-C<sub>3</sub>N<sub>4</sub> structure. Very recently, a new precursor of triazoles has been used to synthesize negatively charged g-C<sub>3</sub>N<sub>4</sub>, and a significantly reduced band gap of 1.5–2.1 eV (responsive to  $\lambda < 590$ –827 nm) was observed.<sup>85</sup> The development of g-C<sub>3</sub>N<sub>4</sub> with a reduced band gap allows the material to harvest and potentially utilize much more solar energy compared with its bare counterpart with a band gap of 2.7 eV (responsive to  $\lambda < 460$  nm). Special attention should be paid to the improved visible light response not being necessarily translated to improved photocatalytic activity, because of the limited oxidizing power of the valence band and reducing power of the conduction band, as discussed in the answer to Question 1.

'OH is the most powerful oxidant in water, 131 and it degrades most organics non-selectively at near diffusion-limited

rates (second-order rate constants of 10<sup>6</sup>-10<sup>10</sup> M<sup>-1</sup> s<sup>-1</sup>). 132-134 In general, it is desired to increase the concentration of 'OH in AOPs for effective contaminant degradation and mineralization, though the strong oxidant 'OH may result in byproduct formation (e.g., bromate<sup>135</sup>). Most g-C<sub>3</sub>N<sub>4</sub> samples have been recognized not to produce 'OH via direct hole oxidation of water since the valence band of most g-C<sub>3</sub>N<sub>4</sub> samples is less positive compared with the reduction potential of OH/H<sub>2</sub>O (2.32 V at pH 7 and 1.99 V at pH 14). Though g-C<sub>3</sub>N<sub>4</sub> is able to produce a series of other ROS (i.e., O<sub>2</sub>-'/ HO2, 1O2, H2O2) or even OH by O2 reduction at the conduction band, the photocatalytic activity for contaminant degradation could be limited due to (i) low reactivity of the other ROS with contaminants (second-order reaction rate constants of  $10^3$ – $10^{10}$  or  $<10^8$  M $^{-1}$  s $^{-1}$  for  $^1O_2$  or  $O_2$ -', $HO_2$ ' with organics)136,137 and (ii) limited production of 'OH. Acid-treated g-C<sub>3</sub>N<sub>4</sub> (protonated) and base-treated g-C<sub>3</sub>N<sub>4</sub> (NaOH doped) were developed in recent studies, and their valence band edges were determined to be 2.37 and 2.27 eV, respectively. 86,87 The shift of the valence band to a more positive energy level could potentially promote the production of 'OH via hole oxidation of water at the valence band. Besides, base-treated g-C<sub>3</sub>N<sub>4</sub> may also have sufficient surface hydroxyl groups that could be activated by photogenerated holes to produce 'OH for photocatalytic reactions. 126

Nanosheets, nanorods, and nanoparticles of g-C<sub>3</sub>N<sub>4</sub> have attracted great attention in recent years because of their significantly increased surface area, charge separation rate, and crystallinity, as mentioned before. 105,138 The quantum confinement effect of nanoscale g-C3N4 shifts the conduction and valence bands in opposite directions and increases the band gap of the material. 139 Its impact on photocatalytic water purification performance could be controversial - the quantum confinement effect increases the redox ability of separated charges for reactions; 90 however, it limits the utilization of visible light of a longer wavelength. Though many nanoscale g-C3N4 samples have been synthesized and characterized to date, experimental and theoretical understanding of how the polymeric structure of triazine units and the length of conjugating units tune the band gap and charge separation of g-C<sub>3</sub>N<sub>4</sub> is still lacking. The polymerization of g-C<sub>3</sub>N<sub>4</sub> building blocks showed an increased UVvisible absorption edge from melamine (235 nm), to melam (285 nm), to melem (296 nm), and to melon (460 nm), which might suggest that the length of conjugating units tailors the band gap.<sup>54</sup> g-C<sub>3</sub>N<sub>4</sub> with different polymeric structures, e.g., poly(triazine imide) and triazine-based g-C3N4, also exhibited distinct band gaps of 2.2 and 1.6-2.0 eV, 140,141 respectively, in contrast to melon (2.7 eV). A systematic approach is needed to prepare, characterize, and simulate nanoscale g-C<sub>3</sub>N<sub>4</sub> with a defined size and shape, and the key parameters can be identified to improve its performance for water purification.

In addition to tailoring the properties of g-C<sub>3</sub>N<sub>4</sub> alone, composites of g-C<sub>3</sub>N<sub>4</sub> with metal nanoparticles (*e.g.*, Au, <sup>142</sup> Ag, <sup>143,144</sup> Pd<sup>145,146</sup>), semiconductors (*e.g.*, TiO<sub>2</sub>, <sup>147-149</sup> ZnO, <sup>150</sup> BiVO<sub>4</sub> <sup>151</sup>), and conductive materials (*e.g.*, carbon nanotubes, <sup>152</sup> graphene oxide, <sup>153,154</sup> carbon nanodots <sup>155-157</sup>) have

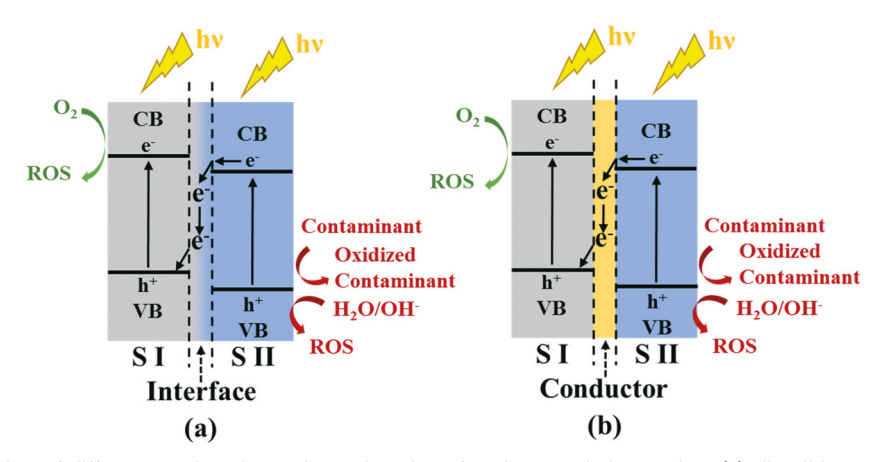


Fig. 6 Schematic illustration of different semiconductor heterojunctions for photocatalytic reaction: (a) all-solid-state semiconductor-semiconductor Z-scheme heterojunction; (b) all-solid-state semiconductor-conductor-semiconductor Z-scheme heterojunction. S I, S II, CB, VB, and ROS represent semiconductor I, semiconductor II, conduction band, valence band, and reactive oxygen species, respectively. The conductor between semiconductors can be metals or carbon.

also been extensively explored. The integration of other functional materials promotes charge separation, increases photon harvesting and utilization, and enhances ROS production. Specifically, g-C<sub>3</sub>N<sub>4</sub> and another semiconductor, with different energy levels of the conduction band and the valence band, are able to form heterojunctions when they are in contact with each other, and an all-solid-state Z-scheme heterojunction attracts great attention because it can harvest low energy photons without compromising the redox ability of photogenerated electrons and holes (Fig. 6). For the Z-scheme heterojunction, photogenerated electrons from semiconductor II with a less-negative conduction band transfer to semiconductor I with a less-positive valence band via direct interfacial contact or a conductive metal as an electron mediator, and are further excited to the conduction band of semiconductor I. Photogenerated holes in semiconductor II are left behind in its valence band. 70 g-C3N4 can be either semiconductor I or II. Though the Z-scheme heterojunction is promising for the improvement of photocatalytic activity, the mechanisms are still not clear.

Future studies should focus on the improvement of photocatalytic performance with a reduced cost of material fabrication, less energy and chemical consumption, and minimized adverse environmental impacts. The mechanistic understanding of improving the charge separation, reducing the band gap, tailoring the band energy levels, ROS production, as well as the Z-scheme heterojunction needs further exploration via the integration of experimental and simulation tools, e.g., advanced material characterization, DFT calculations, molecular dynamics simulations. Notably, theoretical simulations are indispensable as a complementary approach for experiments, and they will significantly advance the knowledge in photocatalysis. Theoretical simulations can be used for rational material design and understanding the key mechanisms that determine the physical, chemical, optical, and electronic properties of g-C<sub>3</sub>N<sub>4</sub>. DFT simulations have been first used to understand the thermochemistry of g-C<sub>3</sub>N<sub>4</sub> in synthesis, and

predict the most thermodynamically stable form of g-C<sub>3</sub>N<sub>4</sub> (melon instead of the graphitic, heptazine-based structure). 52,53 Next, DFT simulations have been applied to understand the molecular structure, band gap, band structure, and charge separation of tailored g-C<sub>3</sub>N<sub>4</sub> samples, including but not limited to doped g-C<sub>3</sub>N<sub>4</sub> (by C, O, P, S), protonated g-C<sub>3</sub>N<sub>4</sub>, g-C<sub>3</sub>N<sub>4</sub> with defects or a distorted structure, g-C<sub>3</sub>N<sub>4</sub> nanosheets, and g-C<sub>3</sub>N<sub>4</sub> composites.  $^{77,80,81,88,108,114,158-165}$ Zheng et al. designed the molecular structure of C- and P-doped g-C<sub>3</sub>N<sub>4</sub> via DFT simulations, predicted the material properties, and compared the band energy levels with the reduction potential of ROS.77 The result suggests that the C-doped but not the P-doped structure can produce ROS under thermodynamically favorable conditions and enhance photocatalytic contaminant degradation. The C-doped structure also localizes holes to improve charge separation. The experimental results, e.g., PL, reaction kinetics of contaminant degradation, were in good agreement with the simulation results, and therefore DFT simulation is a viable tool for rational material design to predict photocatalyst properties and oxidation performance for contaminant removal. Last but not least, DFT and molecular dynamics simulations can predict the adsorption and reaction pathway of contaminants in photocatalysis, 166,167 which will shed light on the mechanism for contaminant removal and further advance the photocatalytic performance for water purification.

### Question 3: how should we appropriately evaluate the photocatalytic performance of g-C<sub>3</sub>N<sub>4</sub>?

The photocatalytic performance of  $g\text{-}C_3N_4$  has been tested in a variety of systems, with different light sources, reactor types, photocatalyst concentrations, contaminants, and water matrices. Table S1† compares the photocatalytic activity of representative  $g\text{-}C_3N_4$ -based photocatalysts; however, it also indicates that a standard approach for reporting the activity is lacking across different research groups. A range of light sources,

including xenon lamps, fluorescent lamps, and light emitting diodes (LEDs), with different light intensities and wavelengths (e.g., visible light  $\lambda > 400$  or 420 nm) have been selected for evaluating the photocatalytic activity. 25,77,168 Under ideal conditions, the quantum yield of a photocatalytic reaction, i.e., the rate of reaction over the rate of photon absorption, should be determined to compare the photocatalytic activities of different photocatalytic systems, because it represents the true reactivity of a photocatalyst. 169 However, the quantum yield is extremely difficult to determine due to the challenges in distinguishing photon absorption from photon scattering and transmission.<sup>39</sup> For most of the time, formal quantum efficiency, i.e., the rate of reaction over the incident light intensity (of either monochromatic or multichromatic light), is used in practice.<sup>39</sup> We recommend measuring and recording the photon fluence and light intensity of the light source, and reporting the photocatalytic activity with respect to the photon fluence (m<sup>2</sup> (mol of photons)<sup>-1</sup>) or light intensity (m<sup>2</sup> J<sup>-1</sup>) instead of pseudo-firstorder reaction rate constants (s<sup>-1</sup>), to facilitate the comparison between different research groups. Most researchers only focus on the reactivity of g-C<sub>3</sub>N<sub>4</sub> under visible light irradiation ( $\lambda$  > 400 or 420 nm); however, its reactivity under UV light irradiation should also be considered, because g-C<sub>3</sub>N<sub>4</sub> can also harvest and utilize UV light for contaminant degradation in practical engineering applications. We recommend testing the photocatalytic activity of g-C<sub>3</sub>N<sub>4</sub> under the irradiation of both visible light and the reference spectrum AM 1.5 that represents the overall yearly average of solar irradiation for mid-latitudes.

Photoreactors with suspended or immobilized g-C<sub>3</sub>N<sub>4</sub> were used for performance evaluation. Slurry reactors with suspended photocatalysts always exhibit an enhanced mass transfer rate; however, quantitative analyses should be conducted to determine whether the measured photocatalytic activity is limited by intraparticle or interparticle mass transfer rates. 77,170,171 The photocatalyst particle size and mixing rate can be tailored to increase the mass transfer rate. The photocatalyst concentration in a slurry reactor may also impact the measured reactivity, and the reaction rate does not necessarily increase proportionally with the increase of the photocatalyst concentration, likely due to the scattering and shielding of photons by the photocatalyst.

It is also very critical to select appropriate contaminants for the photocatalytic activity evaluation. Organic dyes are always selected in the tests: about 85% of studies with a scope of g-C<sub>3</sub>N<sub>4</sub>-based photocatalytic water purification used organic dyes as the only contaminant surrogates, based on our search. However, the dyes may be decomposed under direct photolysis in contrast to photocatalysis.<sup>172</sup> In addition, the dyes may also transfer electrons to the conduction band of g-C<sub>3</sub>N<sub>4</sub> and act as sensitizers under light irradiation (similar to the dyes in dye sensitized solar cells),173-175 which can complicate the interpretation of measured photocatalytic activity. Moreover, some commonly used dyes (e.g., Rhodamine B, methylene blue) are positively charged at circumneutral pH so that they can strongly interact with negatively charged g-C<sub>3</sub>N<sub>4</sub> via electrostatic attraction.<sup>77</sup> In contrast to many contaminants that are neutral or negatively charged (e.g., atrazine, sulfamethoxazole, carbamazepine, bacteria, viruses) at circumneutral pH, the measured photocatalytic activity for positively-charged dyes may over-exaggerate the photocatalytic performance for the degradation of real contaminants. Hence, we strongly do not recommend using dyes as contaminant surrogates for evaluating the photocatalytic performance of g-C<sub>3</sub>N<sub>4</sub>, if the material is considered for water and wastewater treatment. To date, the most widely used contaminant surrogates, excluding organic dyes, for g-C3N4-based photocatalysis are phenolic compounds (e.g., phenol, chlorophenol, nitrophenol) and the antibiotic tetracycline (Table S1†). To best compare the photocatalytic activity across different research laboratories, we recommend selecting multiple contaminants with distinct properties rather than one specific contaminant for degradation, to avoid substrate-specific activity of some photocatalyst samples.77,176

Based on the previous discussion, we propose a standard test system for evaluating the photocatalytic performance of g-C<sub>3</sub>N<sub>4</sub> for contaminant degradation. g-C<sub>3</sub>N<sub>4</sub> synthesized from melamine or dicyandiamide at 550 °C in air, along with TiO<sub>2</sub> P25, can be used as a benchmark photocatalyst for evaluating the performance improvement of tailored, new g-C<sub>3</sub>N<sub>4</sub>. A group of contaminants with different physical and chemical properties (e.g., polarities, charges), not dyes, should be used for the test under the irradiation of both visible light and the reference spectrum AM 1.5 in a model aqueous system. The contaminant concentration, photocatalyst loading, and solution pH and temperature should be kept the same for all tests. A slurry reactor with minimized mass transfer limitation should be considered. The photocatalytic activity should be reported with respect to the photon fluence or light intensity. Table 1 lists one suggested standard test system for evaluating photocatalytic activity.

### Question 4: what key mechanisms are needed to understand the photocatalytic performance of g-C<sub>3</sub>N<sub>4</sub>?

Tailored g-C<sub>3</sub>N<sub>4</sub> properties including an increased surface area, a reduced band gap, a properly positioned band energy level, and improved charge separation have been shown to enhance the photocatalytic performance of g-C<sub>3</sub>N<sub>4</sub>. However, it is challenging to evaluate the contribution of each key property to improved photocatalytic activity, because tailoring an individual g-C<sub>3</sub>N<sub>4</sub> property without changing the others is almost impossible during material synthesis, and some properties are interrelated with each other. For example, g-C<sub>3</sub>N<sub>4</sub> nanosheets, in contrast to their bulk counterpart, always exhibit enhanced photocatalytic activity due to an increased surface area and promoted charge carrier separation. Nevertheless, an increased band gap of the g-C<sub>3</sub>N<sub>4</sub> nanosheets (Fig. 4)<sup>90</sup> could lower their reactivity under visible light irradiation, especially the response to photons with a longer wavelength. Metal and non-metal doping has been shown to improve charge separation and visible light utilization of g-C<sub>3</sub>N<sub>4</sub>; however, the doping sacrifices the material surface area 143,144 and results in the photocatalytic activity

Table 1 A proposed standard system for evaluating photocatalytic activity

Photocatalyst and loading	Contaminants <sup>a</sup>	Contaminant concentration	Water matrix	Light source	Reactor type	Reported reactivity
g- $C_3N_4$ synthesized from melamine or dicyandiamide (1 g $L^{-1}$ )	Phenol	100 μΜ	1 1	Xenon lamp $(\lambda > 400 \text{ nm},$ and AM 1.5	Slurry reactor, minimized mass transfer	Pseudo-first order reaction rates with respect to the photon fluence or light
$TiO_2 P25 (0.1 g L^{-1})$ Tailored g-C <sub>3</sub> N <sub>4</sub> (1 g L <sup>-1</sup> )	Dichloroacetic acid Tetramethylammonium Trichloroethylene		7.0	global)	limitation	intensity

<sup>&</sup>lt;sup>a</sup> Contaminant selection is based on ref. 176. Aromatic, anionic, cationic, and chlorohydrocarbon compounds with distinct molecular properties and structures are chosen.

being difficult to predict. In addition, the doping level should be optimized for improved reactivity because a dopant at a high concentration could become a recombination center for charge carriers. We suggest computational simulations for the mechanistic evaluation of the effect of key material properties on the photocatalytic performance of  $g\text{-}C_3N_4$  on a molecular scale, since the simulations will provide quantitative comparisons that complement experimental analyses and characterization. It is also feasible to tailor the molecular structure of  $g\text{-}C_3N_4$  selectively in the simulations to enable evaluating the contribution of an individual material property to the photocatalytic performance.

Photocatalysis is a complicated AOP because many oxidative species (e.g., ROS and holes) are involved in the reaction, and the concentration of oxidative species and the reactivity between oxidative species and the contaminant (usually characterized by the second-order reaction rate constant) determine the performance for contaminant degradation. TiO2 is a wellcharacterized photocatalyst, and it is known to produce 'OH, either surface bound or water dissolved, for contaminant oxidation.<sup>177</sup> In contrast to conventional TiO<sub>2</sub>, ROS production of g-C<sub>3</sub>N<sub>4</sub> is largely unknown, even though some specific ROS (O<sub>2</sub>-'/HO<sub>2</sub>', <sup>1</sup>O<sub>2</sub>, H<sub>2</sub>O<sub>2</sub>) have been identified to be important in different photocatalytic systems.<sup>55</sup> Specifically, given their conjugated polymer structures, g-C<sub>3</sub>N<sub>4</sub> and its derivatives might involve the transition from the singlet-excited state to the lowerenergy triplet-excited state through intersystem crossing. However, only few studies explored the generation of the tripletexcited state of g-C<sub>3</sub>N<sub>4</sub>, and indicated that the triplet-excited state of g-C<sub>3</sub>N<sub>4</sub> promoted <sup>1</sup>O<sub>2</sub> production. <sup>30</sup> The triplet-excited state of g-C<sub>3</sub>N<sub>4</sub> could also enhance contaminant degradation via electron transfer reactions, similar to chromophoric dissolved organic matter. 178,179 Sorbic acid could be used to determine the concentration of the triplet-excited state and its contribution to photocatalytic reactions. 178,180,181 The reaction of sorbic acid with the triplet-excited state results in the isomerization of sorbic acid, which is unique because the reaction with ROS does not produce isomer products. Future studies should focus on the mechanism of ROS generation and ROScontaminant reaction pathways in g-C<sub>3</sub>N<sub>4</sub> photocatalytic systems, including the contribution of the triplet-excited state.

The second-order reaction rate constant between the contaminant and ROS (in addition to 'OH) is also very critical to understand contaminant degradation or pathogen inactivation via the attack of different ROS, but it is not well-characterized. 180 Probe compounds (PCs) and scavengers/quenchers (S/ Q) are often used to evaluate ROS production (e.g., steady-state concentrations of ROS) and the contribution of one or multiple ROS to contaminant transformation kinetics. 180,182 Competition kinetics experiments, evaluating the kinetics of a specific ROS with the PCs and the contaminant in the same reaction, have been used to determine the second-order reaction rate constant between a specific ROS and the target contaminant because the second-order reaction rate constant of ROS-PC is well-documented. 183-185 The success of these experiments relies on the selective reaction of PCs or S/O with the specific ROS, and the concentrations of PCs and S/Q are also important; the PC concentration has to be sufficiently low to negligibly reduce the steady-state concentration of ROS (µM range), and the S/Q concentration has to be sufficiently high to quench the target ROS without interfering with the reactions between other ROS and the contaminant (mM range). 182 For example, 'OH is highly reactive and non-selective to any PCs, and performance evaluation of ROS other than 'OH should be strategic when 'OH is present, e.g., S/Q can be added into the system to quench undesired 'OH reactions.

Many PCs and S/Q have been developed and used in photocatalytic systems to date. 186 Azide and L-histidine are typical S/Q for 1O2.77,187 Furfuryl alcohol (FFA) is the most widely used PC for <sup>1</sup>O<sub>2</sub>, and its concentration is recommended to be below 110 µM to minimize the interference of added FFA on the steadystate concentration of 1O2. 182 Aliphatic alcohols, e.g., t-butanol and isopropanol, are often used as S/Q for 'OH, and terephthalic acid (TPA) is used as a PC for 'OH because it can form a highly fluorescent product, 2-hydroxyterephthalic acid, during the reaction. 180,182 Other PCs are also used for quantifying 'OH, including coumarin, benzoic acid, and p-chlorobenzoic acid (pCBA), but TPA is advantageous: it is only susceptible to 'OH oxidation rather than direct electron transfer oxidation due to its high activation energy. 188 Using TPA for quantifying 'OH could potentially avoid the interference of other oxidative species (e.g., holes). Benzoquinone (BQ) and superoxide dismutase (SOD), as S/Q, react fast with  $O_2^{-\cdot}$  (second-order reaction rate constants of 10<sup>8</sup>–10<sup>9</sup> M<sup>-1</sup> s<sup>-1</sup>);<sup>77,137,189</sup> however, special attention should be paid when SOD is used because it produces H<sub>2</sub>O<sub>2</sub> that may interfere with photocatalytic reactions. 2-Methyl-6-(4methoxyphenyl)-3,7-dihydroimidazo[1,2-a]pyrazine-3(7H)-one (MCLA), nitro blue tetrazolium chloride (NBT), and 3'-(1-[(phenylamino)-carbonyl]-3,4-tetrazolium)-bis(4-methoxy-6-nitro) benzenesulfonic acid hydrate (XTT) are often used as PCs for  $O_2^{-1}$ . <sup>182,190</sup> The reaction of MCLA- $O_2^{-1}$  results in the emission of a photon at 457 nm for  $O_2^{-1}$  quantification, though it should be a caution that the presence of  $^1O_2$  can interfere with the reaction. <sup>182</sup> NBT or XTT reacting with  $O_2^{-1}$  forms a deep-blue diformazan form that can be quantitatively determined by a colorimetric method. <sup>190</sup>  $H_2O_2$  is a long-lived ROS, and catalase can serve as an S/Q in photocatalytic reactions. <sup>77</sup> The  $H_2O_2$  concentration can be *ex situ* quantified *via* colorimetry, by reacting with *N*,*N*-diethyl-*p*-phenylenediamine (DPD) and horseradish peroxidase to form a pink-colored species. <sup>185</sup>

The most significant challenge remaining in a photocatalytic system, in contrast to a photolysis system, is the evaluation of hole generation and holes-contaminant interaction, because the experimental quantification is difficult, especially in an aqueous solution. To date, the widely used method for analyzing hole generation and the contribution of hole oxidation to contaminant degradation is the quench experiment (e.g., the addition of formic acid<sup>191</sup>); however, the selectivity between the S/Q and the holes in the presence of ROS is not understood. Electrochemical characterization has been recently used to evaluate the contribution of hole oxidation in a photocatalytic reaction via quantitative single-molecule, single-particle fluorescence imaging; however, the sample preparation and experimental set-up are complicated. 192 Holes are much less mobile than electrons and ROS, 99 and contaminant oxidation by the holes is expected to occur on or near the surface of g-C<sub>3</sub>N<sub>4</sub>. Therefore, both contaminant adsorption on g-C<sub>3</sub>N<sub>4</sub> and direct electron transfer from the contaminant to g-C<sub>3</sub>N<sub>4</sub> are critical to determine contaminant oxidation by the holes. Molecular simulations (e.g., DFT and molecular dynamics simulations) are highly promising and viable tools to investigate contaminant oxidation by the holes, including both contaminant adsorption<sup>167</sup> and direct electron transfer kinetics (e.g., transition state of the contaminant, activation energy of oxidation). 193,194

In addition to photocatalytic contaminant degradation, g-C<sub>3</sub>N<sub>4</sub> has also been observed to effectively inactivate microorganisms (e.g., bacteria, viruses) under visible light irradiation. 149,195–198 Therefore, g-C<sub>3</sub>N<sub>4</sub> is believed to hold promise for photocatalytic water disinfection. Though many mechanisms have been proposed for pathogen inactivation, 195,199,200 it is still not clear how g-C<sub>3</sub>N<sub>4</sub> interacts with pathogens and kills them. For example, what is the reaction pathway between the ROS/holes and biomolecules of the pathogen (e.g., lipids, propolysaccharides, deoxyribonucleic acids ribonucleic acids (RNAs))? What mechanism dominates pathogen inactivation, e.g., compromising the structural integrity of the pathogen, interfering with metabolic pathways, preventing pathogen replication, or the combination of any? Bacteria can secrete extracellular polymeric substances (EPS) for developing biofilms, to provide a favorable environment for pathogen survival under stress. Most previous studies of g-C<sub>3</sub>N<sub>4</sub>-based microorganism inactivation were conducted on planktonic bacteria,

and hence there is a need to understand the efficacy and robustness of g-C<sub>3</sub>N<sub>4</sub> for biofilm inactivation.<sup>201-204</sup> Moreover, the unique 2D nanostructure of g-C<sub>3</sub>N<sub>4</sub> may pose additional stress to the pathogens besides that from the ROS/holes. Direct contact between g-C<sub>3</sub>N<sub>4</sub> nanosheets and the pathogen surface (e.g., bacterial membrane, viral capsid or envelope) and/or direct physical penetration or endocytosis of the g-C<sub>3</sub>N<sub>4</sub> nanosheets into the pathogens may lead to pathogen disintegration, membrane function compromise, adverse interactions with biomolecules, and eventually pathogen inactivation, similar to other antimicrobial nanomaterials (e.g., graphene oxide, graphene, nanotubes, transition metal carbides carbonitrides).205-210 We believe molecular simulations can advance the fundamental understanding of biomolecule interactions with g-C<sub>3</sub>N<sub>4</sub>, and the integration of simulations and experimental approaches will provide guidelines for designing g-C<sub>3</sub>N<sub>4</sub> with enhanced performance for pathogen inactivation.

With the development of disinfection for water purification, including photocatalytic disinfection, one concern has emerged: can pathogens develop antioxidant activity in disinfection, similar to antibiotic resistance? It is currently believed that oxidative disinfection attacks multiple targets in pathogens, e.g., proteins, lipids, DNAs, in contrast to antibiotics that usually act on a specific target.<sup>211</sup> Thus, it is much easier for bacteria to develop antibiotic resistance, which could be achieved through target modification. 212 In addition, the disinfection kinetics are fast, and the pathogens may not have sufficient time to overexpress protective proteins (e.g., catalase, superoxide dismutase) to scavenge ROS and protect themselves. Though pathogens are less likely to develop antioxidant activity in disinfection, some 'stronger strains' do exist and they have already acquired genes with intrinsic resistance to oxidative stress. For example, integrative conjugative elements for β-lactam antibiotics and oxidative stress (ICEs-βox) in L. pneumophila promote its resistance to oxidants (e.g., H<sub>2</sub>O<sub>2</sub>, bleach).<sup>213</sup> An MS2 virus exposed to ClO<sub>2</sub>, or even in the absence of ClO<sub>2</sub> pressure, was observed to produce disinfectantresistant strains due to the mutation of ClO2-stable amino acids on the virus capsid and the development of a stable host binding.214 The mechanism of pathogen-ROS/hole interactions and intracellular oxidative stress defense systems is still largely underexplored. Therefore, more thorough studies should be conducted to evaluate the antioxidant activity of pathogens in disinfection, prior to effective and safe implementation of photocatalysis for pathogen inactivation.

# Question 5: what should we pay attention to regarding the engineering applications of g-C<sub>3</sub>N<sub>4</sub> for photocatalytic water purification?

To promote efficient, robust, and safe g-C<sub>3</sub>N<sub>4</sub>-based photocatalytic water purification, we propose to consider and evaluate four aspects of photocatalysis prior to its engineering applications: (i) minimized toxicity and adverse impacts of treated water, (ii) enhanced photocatalytic performance in complex water matrices, (iii) stable long-term performance of the

photocatalyst, and (iv) desired reactor design with improved solar energy utilization for certain water purification scenarios.

g-C<sub>3</sub>N<sub>4</sub> holds promise for removing a broad spectrum of contaminants and pathogens in photocatalysis; however, most efforts were focused on the degradation of parent contaminants and the reduction of pathogen viability in previous studies. In g-C<sub>3</sub>N<sub>4</sub>-based photocatalysis, complete contaminant mineralization may not be realized, likely due to the production of weak ROS (e.g., <sup>1</sup>O<sub>2</sub> and O<sub>2</sub>-',HO<sub>2</sub>') with a lower reduction potential and low reactivity in contrast to 'OH. It is critical to identify the intermediates and by-products in contaminant photocatalytic transformation and the toxicity of these compounds (e.g., mutagenicity, carcinogenicity, genotoxicity), because these compounds may pose risks and adverse impacts to the quality of treated water. Promoting 'OH production for g-C<sub>3</sub>N<sub>4</sub>-based photocatalysis may increase the likelihood of complete contaminant mineralization, <sup>134</sup> and thus eliminate the concerns about toxic intermediates and by-products. Nevertheless, special attention should be paid to limiting by-product formation in the presence of 'OH, such as bromate production. 135 For the photocatalytic inactivation of pathogens, scrutiny of bioactivity degradation beyond pathogen viability should be made. A recent study revealed that full-scale ozonation under typical operational conditions showed negligible degradation of intracellular antibiotic resistance genes (ARGs) for wastewater treatment.215 Similar to ozonation, photocatalysis also takes advantage of ROS oxidation for pathogen inactivation, and may also exhibit limited inactivation of antibiotic resistance activities. Another study even indicated that sublethal stress induced by photocatalysis enhanced ARG transfer among E. coli. 216 Further optimization of g-C<sub>3</sub>N<sub>4</sub>-based photocatalysis (e.g., dosage, light intensity, water quality, material properties) is needed for promoting safe water purification, by minimizing toxic intermediate/by-product production and enhancing bioactivity removal.

The potential toxicity and adverse impacts of g-C<sub>3</sub>N<sub>4</sub> and its daughter products due to self-decomposition in photocatalysis should also be considered. Previous studies, including our preliminary results, have suggested that g-C3N4 is likely to be non-toxic and biocompatible (in the dark), as discussed in the answer to Question 1.67,91 However, detailed, systematic assessment of g-C<sub>3</sub>N<sub>4</sub> is still lacking, and no study reports the toxicity of g-C<sub>3</sub>N<sub>4</sub> daughter products from photocorrosion to date. Analytical instruments can be first used to identify the daughter products of g-C<sub>3</sub>N<sub>4</sub> and their production in photocatalysis. Next, g-C<sub>3</sub>N<sub>4</sub> and its daughter products will be subjected to in vitro and in vivo assessment of their toxicity. In the in vitro assessment, g-C<sub>3</sub>N<sub>4</sub> and its daughter products will be in direct contact with cells, and the interactions with the cells include, but are not limited to, material/chemical uptake and processing, membrane perturbation, and ROS generation.217 Phagocytic cells, including monocyte and macrophage phenotypes, which are the first line of defense in the human body against the invasion of foreign materials/ chemicals, should be chosen for the assessment.218 The timescale and concentration of g-C<sub>3</sub>N<sub>4</sub> and its daughter products in the assessment should be optimized. <sup>219</sup> The *in vivo* assessment mainly focuses on various toxicity, *e.g.*, hematological toxicity, pulmonary toxicity, hepatotoxicity, nephrotoxicity, and splenic toxicity, caused by g-C<sub>3</sub>N<sub>4</sub> and its daughter products. <sup>220</sup> The *in vivo* assessment should model all the potential exposure and investigate the biodistribution profile and the fate of g-C<sub>3</sub>N<sub>4</sub> and its daughter products after ingestion. The timescale of the *in vivo* assessment should be as long as possible, in contrast to that of the *in vitro* assessment, as the result of the *in vivo* assessment could reveal long-term consequences of g-C<sub>3</sub>N<sub>4</sub> and its daughter products. Special attention should be paid to the various structures and morphologies of g-C<sub>3</sub>N<sub>4</sub> on toxicity (*e.g.*, nanosheets).

Many previous studies evaluated the photocatalytic performance of g-C<sub>3</sub>N<sub>4</sub> in a model water matrix, with well-controlled pH and limited impurities. Nevertheless, the presence of natural water constituents, radical scavengers, and foulants may significantly reduce the photocatalytic activity. Water pH may affect the photocatalytic activity for contaminant degradation and pathogen inactivation, likely due to the impact of the surface interaction of g-C<sub>3</sub>N<sub>4</sub> and contaminants/pathogens, thermodynamics of ROS production, and reaction kinetics between ROS and the contaminants/pathogens. Many g-C<sub>3</sub>N<sub>4</sub> samples are negatively charged at circumneutral pH,77,158,221 and their adsorption to and oxidation of positively charged contaminants are expected to be favorable. pH also tailors ROS production, e.g., 'OH formation from direct hole oxidation of H2O becomes thermodynamically favorable at elevated pH, based on the Nernst equation. In addition, the reaction kinetics of ROS with contaminants are also dependent on pH; oxidation of protonated (substituted) phenols by <sup>1</sup>O<sub>2</sub> is ca. 10-100 times slower than that of their phenolate counterparts, based on the second-order reaction rate constant.<sup>222</sup> Dissolved oxygen is another important water quality parameter that determines ROS production and subsequent contaminant degradation or pathogen inactivation, 223 and photocatalytic kinetics is always inhibited with limited oxygen supply. Natural organic matter (NOM) can strongly bind to and foul the surface of some photocatalysts (e.g., TiO2).224 Moreover, NOM competes with contaminants/pathogens for the reaction with ROS (e.g., competition for 'OH because 'OH oxidation is non-selective), 134,225,226 and thus the presence of NOM could significantly reduce the photocatalytic activity for contaminant degradation and pathogen inactivation. Radical scavengers (e.g., CO<sub>3</sub><sup>2-</sup>, HS<sup>-</sup>) in water also quench ROS or produce radicals with lower reactivity (e.g., CO3-) and reduce the reaction rate for contaminant and pathogen removal. Our previous study was the first one to systematically evaluate the performance of g-C<sub>3</sub>N<sub>4</sub> in simulated and real complex water matrices, and we did not observe any reactivity inhibition across a variety of water chemistries representative of drinking water and wastewater treatment.<sup>77</sup> The promising results indicated that the g-C<sub>2</sub>N<sub>4</sub> samples in our study were not susceptible to the water impurities; however, further mechanistic understanding is needed to evaluate future g-C<sub>3</sub>N<sub>4</sub> samples in complex water matrices.



Fig. 7 Compound parabolic collectors (CPCs) for photocatalytic water purification on a pilot scale or an industrial scale. Indirect light is reflected by the parabolic collectors onto the absorber tube surface at the center. Photocatalysts, either suspended in water or immobilized on a tube surface, facilitate contaminant degradation or disinfection under solar irradiation. Water is recirculated through the tubes for treatment. Suspended photocatalysts require post-separation after treatment. Reproduced from ref. 235 with permission from Elsevier.

The long-term performance of g-C<sub>3</sub>N<sub>4</sub> should be evaluated before its implementation for water purification. Photocorrosion due to photocatalyst self-oxidation, photocatalyst fouling and regeneration, and mass loss of the photocatalyst in water purification need to be considered. The photostability of g-C<sub>3</sub>N<sub>4</sub> should be evaluated under continuous light irradiation, and the structure, morphology, elemental composition, surface functional groups, oxidation state and bonding environment, and transformation products should be characterized. This photocatalyst can prevent the fouling of organic substances (e.g., NOM) or biofilms, because of the generation of highly reactive ROS for the oxidation of organics and the inactivation of microorganisms. 21,22,224 Nevertheless, metal adsorption, mineral precipitation (e.g., hardness species), and inorganic particle/colloid fouling can decrease its photocatalytic activity.<sup>227</sup> Physical and chemical cleaning and regeneration could be used to restore the reactivity of the photocatalyst. 228 The mass loss of g-C<sub>3</sub>N<sub>4</sub> should be prevented in water purification; efficient post-separation can improve photocatalyst retaining in a slurry reactor, or a strong photocatalyst-support interaction and water flow with desired shear stress can keep the photocatalyst immobilized in the reactor.

Centralized, large-scale water treatment systems with the implementation of photocatalysis could require either high energy consumption when artificial light is used or high reactor footprint when sunlight is used.<sup>229</sup> Small-scale water treatment systems, including small public water systems (PWS) and point-of-entry (POE) and point-of-use (POU) treatment devices, also serve a large number of U.S. populations.<sup>230</sup> However, due to limited financial resources and operational capacity, small-scale water treatment systems are more likely to violate drinking water regulations than centralized, large PWS, 11,230-233 and the presence of persistent and emerging chemical and biological contaminants further challenges the safety of treated water. Photocatalysis for small-scale water treatment provides high quality treated water, reduces energy and chemical consumption, and requires decent footprint, and we believe its application is desired for rural areas, small communities, single households, and developing countries. Photocatalysis is also suitable for smallscale advanced wastewater treatment for water reuse. Last

but not least, photocatalytic reactor design remains as a major barrier to preventing the industrial application of photocatalysis, and hence the development and optimization of reactors are urgently needed. To date, a variety of photoreactors have been proposed, such as parabolic trough reactors, compound parabolic collectors (CPCs, Fig. 7), inclined plate collectors, double-skin sheet reactors, and rotating disk reactors.234 CPCs are most suited to pilot-scale or industrial-scale applications (>1000 L per day) due to their high collection rate of solar radiation and well-known reactor design methodology,38,234,235 and they have been successfully used for the photocatalytic degradation of PPCPs, pesticides, and industrial chemicals, as well as disinfection. 236-243 Industrial-scale studies (i.e., reactor size up to 800 L, solar collection area up to 100 m<sup>2</sup>) have demonstrated the viability of CPCs for the photocatalytic destruction of contaminants and disinfection for small PWS or POE applications. 244-246 The performance of g-C<sub>3</sub>N<sub>4</sub> in CPCs should be evaluated for potential industrial-scale photocatalytic applications, and further optimization of CPCs as well as the development of photoreactors beyond current paradigms with improved solar energy utilization, mass transfer rate, photocatalyst separation, and water treatment capacity is highly desired.

### Conclusion, perspective, and outlook

g-C<sub>3</sub>N<sub>4</sub> is an emerging visible-light-responsive photocatalyst that has attracted attention for sustainable water purification in recent years. This material is believed to have several merits that are ideal for water purification; it is synthesized from earth-abundant precursors, stable, biocompatible with no reported toxicity, and has highly tunable structures and properties to enhance solar energy utilization and photocatalytic performance for degrading persistent and emerging contaminants. Most previous studies were focused on the synthesis and characterization of g-C<sub>3</sub>N<sub>4</sub> to understand how to tailor the material properties to enhance its reactivity. The band gap is an important optical parameter of g-C<sub>3</sub>N<sub>4</sub>, and it determines the amount of solar energy that the material can harvest and use. A reduced band gap corresponds to an extended use of visible photons at a longer wavelength;

however, band energy levels have to maintain sufficient thermodynamic driving force for ROS production (especially 'OH) and the resulting contaminant degradation and pathogen inactivation. Charge separation needs to be enhanced to provide more charge carriers for effective photocatalytic reactions. The increase of the g-C<sub>3</sub>N<sub>4</sub> surface area by creating a porous or nanoscale structure not only improves charge separation but also provides more available sites for the reactions. The creation of a Z-scheme heterojunction of g-C<sub>3</sub>N<sub>4</sub> with another photocatalyst can promote charge separation and utilize low-energy visible photons without compromising the redox ability of photogenerated electrons and holes. Theoretical simulations, e.g., DFT and molecular dynamics simulations, can predict the molecular structure, properties, and photocatalytic performance of g-C<sub>3</sub>N<sub>4</sub> for contaminant degradation, and the simulations can provide a guideline for rational material design prior to the synthesis.

A standard approach is needed to compare the photocatalytic performance of  $g\text{-}C_3N_4$  across different research groups. Organic dyes should not be used as contaminant surrogates, and real contaminants are recommended for photocatalytic tests. Multiple contaminants with distinct properties should be used to avoid substrate-specific activity. Bulk  $g\text{-}C_3N_4$  synthesized from the thermal polycondensation of melamine and dicyandiamide can be used as the benchmark for photocatalytic activity comparison, and the catalyst loading, light source and intensity, contaminant concentration, water matrix, and reactor type should be specified. The measured photocatalytic activity should be reported with respect to the photon fluence or light intensity.

To understand the mechanism of photocatalytic reactions with waterborne contaminants and pathogens, the amount and type of oxidative species, *e.g.*, ROS, holes, triplet-excited state, and their contribution to photocatalytic reaction kinetics should be determined. PCs can be used to quantify the concentration of these oxidative species, and the addition of S/Q can shed light on the significance of oxidative species in the reactions. Special attention should be paid to the reaction specificity between one oxidative species and its corresponding PCs or S/Q. The experimental understanding of holescontaminant/pathogen interactions is challenging, and theoretical simulations are viable tools to provide insights.

To improve the effectiveness, robustness, and safety of  $g\text{-}C_3N_4\text{-}\text{based}$  photocatalytic water purification, we will need to evaluate the following aspects prior to engineering applications. First, the scalable production, photostability, and recyclability of the photocatalyst should be evaluated. The  $g\text{-}C_3N_4$  yield from its precursors should be increased to improve the atom economy, and thus reduce the cost for material development. The photostability of  $g\text{-}C_3N_4$  needs to be explored systematically to improve the long-term use of this material. Enhanced separation of  $g\text{-}C_3N_4$  from treated water or  $g\text{-}C_3N_4$  immobilization in the reactor will promote the recyclability of the photocatalyst for continuous use. Second, the long-term performance of the photocatalyst in complex water matrices requires further understanding, by exploring the effect

of pH, natural water constituents, radical scavengers, and foulants (especially inorganics) on photocatalytic activity. Third, the environmental impacts of treated water are critical for a safe water supply, and the toxicity of the photocorrosion by-products of g-C<sub>3</sub>N<sub>4</sub>, the toxicity of contaminant degradation products, and pathogen bioactivities (e.g., viability, antibiotic resistance, antioxidant activity) should be minimized for the treated water. Last but not least, CPC photoreactors are most suitable for pilot- and industrial-scale water purification to date; nevertheless, photoreactor design needs to be further advanced and optimized for enhanced solar energy utilization, mass transfer rates, photocatalyst separation, and water treatment performance. The commercialization of the photocatalyst and photoreactor is also important for future mass deployment of the technology. g-C<sub>3</sub>N<sub>4</sub>-based photocatalysis is ideal for sustainable small-scale water treatment in rural areas, small communities, single households, and developing countries, and it is promising to generate high quality treated water, utilize inexhaustible renewable solar energy, and reduce the capital, operation, and maintenance cost of water practice.

### Acknowledgements

We thank the National Science Foundation Grant CBET-1437989 and CBET-1604886 for financial support. We also thank the start-up grant of the Department of Civil and Environmental Engineering, The George Washington University for financial support.

### References

- 1 Occurrence of contaminants of emerging concern in wastewater from nine publicly owned treatment works, EPA 821-R-09-009, Office of Water, U.S. Environmental Protection Agency, Washington, DC, 2009.
- 2 Treating contaminants of emerging concern: A literature review database, EPA-820-R-10-002, Office of Water, U.S. Environmental Protection Agency, Washington, DC, 2010.
- 3 *Pharmaceuticals in drinking-water*, World Health Organization, Geneva, Switzerland, 2012.
- 4 New Science Challenges Old Assumptions about Harmful Algal Blooms, https://www.usgs.gov/news/new-science-challenges-old-assumptions-about-harmful-algal-blooms, (accessed Jul 6, 2017).
- 5 J. Lan, M. Hu, C. Gao, A. Alshawabkeh and A. Z. Gu, Environ. Sci. Technol., 2015, 49, 6284–6293.
- 6 A. M. Dietrich, A. Thomas, Y. Zhao, E. Smiley, N. Shanaiah, M. Ahart, K. A. Charbonnet, N. J. DeYonker, W. A. Alexander and D. L. Gallagher, *Environ. Sci. Technol. Lett.*, 2015, 2, 123–127.
- 7 A. J. Whelton, L. McMillan, M. Connell, K. M. Kelley, J. P. Gill, K. D. White, R. Gupta, R. Dey and C. Novy, *Environ. Sci. Technol.*, 2015, 49, 813–823.
- 8 K. M. Parker, T. Zeng, J. Harkness, A. Vengosh and W. A. Mitch, *Environ. Sci. Technol.*, 2014, 48, 11161–11169.

- 9 K. Bibby, L. W. Casson, E. Stachler and C. N. Haas, *Environ. Sci. Technol. Lett.*, 2014, 2, 2–6.
- 10 K. R. Wigginton, Y. Ye and R. M. Ellenberg, *Environ. Sci.:* Water Res. Technol., 2015, 1, 735–746.
- 11 G. F. Craun, J. M. Brunkard, J. S. Yoder, V. A. Roberts, J. Carpenter, T. Wade, R. L. Calderon, J. M. Roberts, M. J. Beach and S. L. Roy, *Clin. Microbiol. Rev.*, 2010, 23, 507–528.
- 12 R. L. Oulton, T. Kohn and D. M. Cwiertny, *J. Environ. Monit.*, 2010, 12, 1956–1978.
- 13 R. Jones, B. Wills and C. Kang, West J. Emerg. Med., 2009, 11, 151–156.
- 14 J. Shah and N. Qureshi, Opflow, 2008, 34, 24-27.
- 15 R. S. Raucher and J. E. Cromwell, *Risks and Benefits of Energy Management for Drinking Water Utilities*, AWWA Research Foundation, 2008.
- 16 M. N. Chong, B. Jin, C. W. Chow and C. Saint, Water Res., 2010, 44, 2997–3027.
- 17 D. Friedmann, C. Mendive and D. Bahnemann, *Appl. Catal.*, *B*, 2010, **99**, 398–406.
- 18 M. H. Prez, G. Peuela, M. I. Maldonado, O. Malato, P. Fernndez-Ibez, I. Oller, W. Gernjak and S. Malato, Appl. Catal., B, 2006, 64, 272–281.
- 19 M. G. Antoniou, J. A. Shoemaker, A. A. de la Cruz and D. D. Dionysiou, *Environ. Sci. Technol.*, 2008, 42, 8877–8883.
- 20 N. G. Chorianopoulos, D. S. Tsoukleris, E. Z. Panagou, P. Falaras and G. Nychas, *Food Microbiol.*, 2011, 28, 164–170.
- 21 M. Raulio, V. Pore, S. Areva, M. Ritala, M. Leskel, M. Lindn, J. B. Rosenholm, K. Lounatmaa and M. Salkinoja-Salonen, J. Ind. Microbiol. Biotechnol., 2006, 33, 261–268.
- 22 S. Ciston, R. M. Lueptow and K. A. Gray, J. Membr. Sci., 2009, 342, 263–268.
- 23 M. R. Hoffmann, S. T. Martin, W. Y. Choi and D. W. Bahnemann, *Chem. Rev.*, 1995, 95, 69–96.
- 24 H. Wang, Y. Su, H. Zhao, H. Yu, S. Chen, Y. Zhang and X. Quan, *Environ. Sci. Technol.*, 2014, 48, 11984–11990.
- 25 F. Dong, Z. Wang, Y. Li, W. Ho and S. C. Lee, *Environ. Sci. Technol.*, 2014, **48**, 10345–10353.
- 26 X. Wang, K. Maeda, A. Thomas, K. Takanabe, G. Xin, J. M. Carlsson, K. Domen and M. Antonietti, *Nat. Mater.*, 2009, 8, 76–80.
- 27 M. Long, W. Cai, J. Cai, B. Zhou, X. Chai and Y. Wu, *J. Phys. Chem. B*, 2006, 110, 20211–20216.
- 28 J. Kim, C. W. Lee and W. Choi, *Environ. Sci. Technol.*, 2010, 44, 6849–6854.
- 29 G. Mamba and A. K. Mishra, *Appl. Catal.*, *B*, 2016, 198, 347–377.
- 30 H. Wang, S. Jiang, S. Chen, D. Li, X. Zhang, W. Shao, X. Sun, J. Xie, Z. Zhao and Q. Zhang, *Adv. Mater.*, 2016, 28, 6940–6945.
- 31 Y. Nosaka and A. Y. Nosaka, *Photocatalysis and Water Purification*, ed. P. Pichat, Wiley-VCH Verlag GmbH & Co. KGaA, Weinheim, Germany, 2013, pp. 1–24.
- 32 P. M. Wood, Biochem. J., 1988, 253, 287-289.
- 33 W. H. Koppenol, Nature, 1976, 262, 420-421.
- 34 Y. Ma, X. Wang, Y. Jia, X. Chen, H. Han and C. Li, *Chem. Rev.*, 2014, 114, 9987–10043.

- 35 M. Darbandi, T. Gebre, L. Mitchell, W. Erwin, R. Bardhan, M. D. Levan, M. D. Mochena and J. H. Dickerson, *Nanoscale*, 2014, 6, 5652–5656.
- 36 W. Ong, L. Tan, S. Chai, S. Yong and A. R. Mohamed, ChemSusChem, 2014, 7, 690-719.
- 37 C. P. Sajan, S. Wageh, A. Al-Ghamdi, J. Yu and S. Cao, *Nano Res.*, 2016, 9, 3–27.
- 38 D. A. Keane, K. G. McGuigan, P. F. Ibez, M. I. Polo-Lpez, J. A. Byrne, P. S. Dunlop, K. O'Shea, D. D. Dionysiou and S. C. Pillai, *Catal. Sci. Technol.*, 2014, 4, 1211–1226.
- 39 M. Pelaez, N. T. Nolan, S. C. Pillai, M. K. Seery, P. Falaras, A. G. Kontos, P. S. M. Dunlop, J. W. J. Hamilton, J. A. Byrne, K. O'Shea, M. H. Entezari and D. D. Dionysiou, *Appl. Catal.*, B, 2012, 125, 331–349.
- 40 G. Huang, Z. Ma, W. Huang, Y. Tian, C. Jiao, Z. Yang, Z. Wan and A. Pan, *J. Nanomater.*, 2013, 2013, 1–8.
- 41 Z. Huang, L. Pan, J. Zou, X. Zhang and L. Wang, *Nanoscale*, 2014, 6, 14044–14063.
- 42 L. Ye, Y. Su, X. Jin, H. Xie and C. Zhang, *Environ. Sci.: Nano*, 2014, 1, 90–112.
- 43 S. C. Lo, C. F. Lin, C. H. Wu and P. H. Hsieh, J. Hazard. Mater., 2004, 114, 183–190.
- 44 A. H. Zyoud, N. Zaatar, I. Saadeddin, C. Ali, D. Park, G. Campet and H. S. Hilal, *J. Hazard. Mater.*, 2010, 173, 318–325.
- 45 E. L. Cates, S. L. Chinnapongse, J. Kim and J. Kim, *Environ. Sci. Technol.*, 2012, 46, 12316–12328.
- 46 Y. Hu, X. Gao, L. Yu, Y. Wang, J. Ning, S. Xu and X. W. Lou, *Angew. Chem., Int. Ed.*, 2013, 52, 5636–5639.
- 47 D. M. Teter and R. J. Hemley, Science, 1996, 271, 53.
- 48 J. Liebig, Ann. Pharm., 1834, 10, 10.
- 49 Y. Wang, X. Wang and M. Antonietti, *Angew. Chem., Int. Ed.*, 2012, 51, 68–89.
- 50 F. Goettmann, A. Fischer, M. Antonietti and A. Thomas, *Chem. Commun.*, 2006, 4530–4532.
- 51 Y. Zheng, J. Liu, J. Liang, M. Jaroniec and S. Z. Qiao, *Energy Environ. Sci.*, 2012, 5, 6717–6731.
- 52 T. Botari, W. P. Huhn, V. W. Lau, B. V. Lotsch and V. Blum, *Chem. Mater.*, 2017, 29, 4445–4453.
- 53 S. T. Melissen, S. N. Steinmann, T. Le Bahers and P. Sautet, J. Phys. Chem. C, 2016, 120, 24542–24550.
- 54 F. K. Kessler, Y. Zheng, D. Schwarz, C. Merschjann, W. Schnick, X. Wang and M. J. Bojdys, *Nat. Rev. Mater.*, 2017, 2, 17030.
- 55 W. Ong, L. Tan, Y. H. Ng, S. Yong and S. Chai, *Chem. Rev.*, 2016, 116, 7159–7329.
- 56 W. Ong, L. Tan, S. Chai and S. Yong, Chem. Commun., 2015, 51, 858-861.
- 57 H. Ou, L. Lin, Y. Zheng, P. Yang, Y. Fang and X. Wang, Adv. Mater., 2017, 29, 1700008.
- 58 W. Ong, L. Tan, S. Chai and S. Yong, *Dalton Trans.*, 2015, 44, 1249–1257.
- 59 W. Ong, L. K. Putri, L. Tan, S. Chai and S. Yong, Appl. Catal., B, 2016, 180, 530–543.
- 60 Z. Pan, Y. Zheng, F. Guo, P. Niu and X. Wang, *ChemSusChem*, 2017, **10**, 87–90.

- 61 W. Ong, L. K. Putri, Y. Tan, L. Tan, N. Li, Y. H. Ng, X. Wen and S. Chai, *Nano Res.*, 2017, 10, 1673–1696.
- 62 B. Long, Y. Zheng, L. Lin, K. A. Alamry, A. M. Asiri and X. Wang, J. Mater. Chem. A, 2017, DOI: 10.1039/C6TA09802A.
- 63 J. Zhu, P. Xiao, H. Li and S. A. Carabineiro, ACS Appl. Mater. Interfaces, 2014, 6, 16449–16465.
- 64 Y. Wang, L. Li, Y. Wei, J. Xue, H. Chen, L. Ding, J. Caro and H. Wang, *Angew. Chem.*, *Int. Ed.*, 2017, 56, 8974–8980.
- 65 S. Barman and M. Sadhukhan, J. Mater. Chem., 2012, 22, 21832–21837.
- 66 J. Tian, Q. Liu, A. M. Asiri, A. O. Al-Youbi and X. Sun, *Anal. Chem.*, 2013, 85, 5595–5599.
- 67 X. Zhang, X. Xie, H. Wang, J. Zhang, B. Pan and Y. Xie, J. Am. Chem. Soc., 2012, 135, 18–21.
- 68 J. Bian, C. Huang and R. Zhang, *ChemSusChem*, 2016, 9, 2723-2735.
- 69 J. Liu, H. Wang and M. Antonietti, Chem. Soc. Rev., 2016, 45, 2308–2326.
- 70 S. Cao, J. Low, J. Yu and M. Jaroniec, Adv. Mater., 2015, 27, 2150–2176.
- 71 S. Dong, J. Feng, M. Fan, Y. Pi, L. Hu, X. Han, M. Liu, J. Sun and J. Sun, *RSC Adv.*, 2015, 5, 14610–14630.
- 72 G. Zhang, Z. Lan and X. Wang, *Chem. Sci.*, 2017, 8, 5261–5274.
- 73 Y. Zheng, L. Lin, B. Wang and X. Wang, Angew. Chem., Int. Ed., 2015, 54, 12868–12884.
- 74 W. Ong, Front. Mater., 2017, 4, 11.
- 75 L. Zhou, H. Zhang, H. Sun, S. Liu, M. O. Tade, S. Wang and W. Jin, *Catal. Sci. Technol.*, 2016, 6, 7002–7023.
- 76 F. Ding, D. Yang, Z. Tong, Y. Nan, Y. Wang, X. Zou and Z. Jiang, *Environ. Sci.: Nano*, 2017, 4, 1455–1469.
- 77 Q. Zheng, D. P. Durkin, J. E. Elenewski, Y. Sun, N. A. Banek, L. Hua, H. Chen, M. J. Wagner, W. Zhang and D. Shuai, *Environ. Sci. Technol.*, 2016, 50, 12938–12948.
- 78 S. M. Aspera, H. Kasai and H. Kawai, *Surf. Sci.*, 2012, **606**, 892–901.
- 79 J. Hong, X. Xia, Y. Wang and R. Xu, *J. Mater. Chem.*, 2012, 22, 15006–15012.
- 80 J. Ran, T. Y. Ma, G. Gao, X. Du and S. Z. Qiao, *Energy Environ. Sci.*, 2015, 8, 3708–3717.
- 81 G. Dong, K. Zhao and L. Zhang, *Chem. Commun.*, 2012, 48, 6178–6180.
- 82 J. Li, B. Shen, Z. Hong, B. Lin, B. Gao and Y. Chen, *Chem. Commun.*, 2012, 48, 12017–12019.
- 83 S. C. Yan, Z. S. Li and Z. G. Zou, *Langmuir*, 2010, 26, 3894–3901.
- 84 Y. Cui, Z. Ding, X. Fu and X. Wang, Angew. Chem., Int. Ed., 2012, 51, 11814–11818.
- 85 D. Dontsova, S. Pronkin, M. Wehle, Z. Chen, C. Fettkenhauer, G. Clavel and M. Antonietti, *Chem. Mater.*, 2015, 27, 5170–5179.
- 86 J. Zhang, S. Hu and Y. Wang, RSC Adv., 2014, 4, 62912–62919.
- 87 C. Ye, J. Li, Z. Li, X. Li, X. Fan, L. Zhang, B. Chen, C. Tung and L. Wu, *ACS Catal.*, 2015, 5, 6973–6979.

- 88 X. Ma, Y. Lv, J. Xu, Y. Liu, R. Zhang and Y. Zhu, *J. Phys. Chem. C*, 2012, **116**, 23485–23493.
- 89 X. Du, G. Zou, Z. Wang and X. Wang, *Nanoscale*, 2015, 7, 8701–8706.
- 90 P. Niu, L. Zhang, G. Liu and H. Cheng, Adv. Funct. Mater., 2012, 22, 4763–4770.
- 91 M. Ayan-Varela, S. Villar-Rodil, J. I. Paredes, J. M. Munuera, A. Pagan, A. A. Lozano-Perez, J. L. Cenis, A. Martinez-Aonso and J. M. D. Tascon, ACS Appl. Mater. Interfaces, 2015, 7, 24032–24045.
- 92 F. Z. Cui and D. J. Li, Surf. Coat. Technol., 2000, 131, 481-487.
- 93 P. Y. Tessier, L. Pichon, P. Villechaise, P. Linez, B. Angleraud, N. Mubumbila, V. Fouquet, A. Straboni, X. Milhet and H. F. Hildebrand, *Diamond Relat. Mater.*, 2003, 12, 1066–1069.
- 94 J. Zhang, X. Chen, K. Takanabe, K. Maeda, K. Domen, J. D. Epping, X. Fu, M. Antonietti and X. Wang, *Angew. Chem.*, *Int. Ed.*, 2010, 49, 441–444.
- 95 Y. Cui, Z. Ding, P. Liu, M. Antonietti, X. Fu and X. Wang, Phys. Chem. Chem. Phys., 2012, 14, 1455–1462.
- 96 G. R. Bamwenda and H. Arakawa, Appl. Catal., A, 2001, 210, 181–191.
- 97 S. Kohtani, K. Yoshida, T. Maekawa, A. Iwase, A. Kudo, H. Miyabe and R. Nakagaki, *Phys. Chem. Chem. Phys.*, 2008, 10, 2986–2992.
- 98 X. Yang, H. Tang, J. Xu, M. Antonietti and M. Shalom, *ChemSusChem*, 2015, 8, 1350–1358.
- 99 S. Fonash, Solar Cell Device Physics, Academic Press, 2010.
- 100 J. Lin, Z. Pan and X. Wang, ACS Sustainable Chem. Eng., 2013, 2, 353–358.
- 101 T. Sano, S. Tsutsui, K. Koike, T. Hirakawa, Y. Teramoto, N. Negishi and K. Takeuchi, J. Mater. Chem. A, 2013, 1, 6489–6496.
- 102 Inventory of Effective Food Contact Substance (FCS) Notifications, http://www.accessdata.fda.gov/scripts/fdcc/? set=fcn, (accessed Jul 6, 2017).
- 103 Y. Yuan, L. Zhang, J. Xing, M. I. B. Utama, X. Lu, K. Du, Y. Li, X. Hu, S. Wang and A. Gen, *Nanoscale*, 2015, 7, 12343–12350.
- 104 X. Lu, K. Xu, P. Chen, K. Jia, S. Liu and C. Wu, J. Mater. Chem. A, 2014, 2, 18924–18928.
- 105 J. Zhang, Y. Chen and X. Wang, *Energy Environ. Sci.*, 2015, 8, 3092–3108.
- 106 S. Yang, Y. Gong, J. Zhang, L. Zhan, L. Ma, Z. Fang, R. Vajtai, X. Wang and P. M. Ajayan, Adv. Mater., 2013, 25, 2452–2456.
- 107 J. Zhang, F. Guo and X. Wang, Adv. Funct. Mater., 2013, 23, 3008–3014.
- 108 P. Niu, L. Yin, Y. Yang, G. Liu and H. Cheng, *Adv. Mater.*, 2014, 26, 8046–8052.
- 109 Q. Tay, P. Kanhere, C. F. Ng, S. Chen, S. Chakraborty, A. C. H. Huan, T. C. Sum, R. Ahuja and Z. Chen, *Chem. Mater.*, 2015, 27, 4930–4933.
- 110 Q. Liang, Z. Li, Z. Huang, F. Kang and Q. Yang, *Adv. Funct. Mater.*, 2015, 25, 6885–6892.

- 111 P. Yang, J. Zhao, W. Qiao, L. Li and Z. Zhu, *Nanoscale*, 2015, 7, 18887–18890.
- 112 W. Ho, Z. Zhang, M. Xu, X. Zhang, X. Wang and Y. Huang, *Appl. Catal.*, *B*, 2015, 179, 106–112.
- 113 Y. Kang, Y. Yang, L. Yin, X. Kang, G. Liu and H. Cheng, *Adv. Mater.*, 2015, 27, 4572–4577.
- 114 X. Zhang, X. Xie, H. Wang, J. Zhang, B. Pan and Y. Xie, J. Am. Chem. Soc., 2012, 135, 18–21.
- 115 M. Rong, L. Lin, X. Song, Y. Wang, Y. Zhong, J. Yan, Y. Feng, X. Zeng and X. Chen, *Biosens. Bioelectron.*, 2015, 68, 210–217.
- 116 X. Cao, J. Ma, Y. Lin, B. Yao, F. Li, W. Weng and X. Lin, *Spectrochim. Acta, Part A*, 2015, 151, 875–880.
- 117 Y. Tang, Y. Su, N. Yang, L. Zhang and Y. Lv, *Anal. Chem.*, 2014, 86, 4528–4535.
- 118 J. Wu, S. Yang, J. Li, Y. Yang, G. Wang, X. Bu, P. He, J. Sun, J. Yang, Y. Deng, G. Ding and X. Xie, Adv. Opt. Mater., 2016, 4, 2095–2101.
- 119 Y. Lu, J. Chen, A. Wang, N. Bao, J. Feng, W. Wang and L. Shao, *J. Mater. Chem. C*, 2015, 3, 73–78.
- 120 J. Zhou, Y. Yang and C. Zhang, Chem. Commun., 2013, 49, 8605–8607.
- 121 J. R. Lakowicz, Principles of fluorescence spectroscopy, Springer US, 2013.
- 122 M. Grabolle, M. Spieles, V. Lesnyak, N. Gaponik, A. Eychmüller and U. Resch-Genger, *Anal. Chem.*, 2009, 81, 6285–6294.
- 123 M. Shalom, S. Inal, C. Fettkenhauer, D. Neher and M. Antonietti, J. Am. Chem. Soc., 2013, 135, 7118-7121.
- 124 M. Shalom, M. Guttentag, C. Fettkenhauer, S. Inal, D. Neher, A. Llobet and M. Antonietti, *Chem. Mater.*, 2014, 26, 5812–5818.
- 125 Z. Huang, F. Li, B. Chen and G. Yuan, *ChemSusChem*, 2016, 9, 478–484.
- 126 Y. Li, S. Ouyang, H. Xu, X. Wang, Y. Bi, Y. Zhang and J. Ye, *J. Am. Chem. Soc.*, 2016, 138, 13289–13297.
- 127 Q. Lin, L. Li, S. Liang, M. Liu, J. Bi and L. Wu, *Appl. Catal.*, *B*, 2015, **163**, 135–142.
- 128 X. Fan, L. Zhang, R. Cheng, M. Wang, M. Li, Y. Zhou and J. Shi, *ACS Catal.*, 2015, 5, 5008–5015.
- 129 X. Li, G. Hartley, A. J. Ward, P. A. Young, A. F. Masters and T. Maschmeyer, *J. Phys. Chem. C*, 2015, **119**, 14938–14946.
- 130 Q. Gu, Z. Gao and C. Xue, Small, 2016, 12, 3543-3549.
- 131 J. Staehelin and J. Hoigne, Environ. Sci. Technol., 1985, 19, 1206–1213.
- 132 P. Neta and L. M. Dorfman, in *Radiation Chemistry*, ed. E. Hart, American Chemical Society, 1968, vol. 16, pp. 222–230.
- 133 W. R. Haag and C. C. D. Yao, *Environ. Sci. Technol.*, 1992, 26, 1005-1013.
- 134 M. G. Antoniou, C. Zhao, K. E. O'Shea, G. Zhang, D. D. Dionysiou, C. Zhao, C. Han, M. N. Nadagouda, H. Choi, T. Fotiou, T. M. Triantis and A. Hiskia, in *Photocatalysis: Applications*, ed. D. Dionysiou, G. Puma, J. Ye, J. Schneider and D. Bahnemann, Royal Society of Chemistry, Croydon, CR0 4YY, UK, 2016, pp. 1–34.
- 135 U. Vongunten and J. Holgne, *Environ. Sci. Technol.*, 1994, 28, 1234–1242.

- 136 F. Wilkinson, W. P. Helman and A. B. Ross, J. Phys. Chem. Ref. Data, 1995, 24, 663–677.
- 137 B. H. J. Bielski, D. E. Cabelli, R. L. Arudi and A. B. Ross, J. Phys. Chem. Ref. Data, 1985, 14, 1041–1100.
- 138 X. Li, J. Zhang, X. Chen, A. Fischer, A. Thomas, M. Antonietti and X. Wang, *Chem. Mater.*, 2011, 23, 4344–4348.
- 139 J. D. Moras, B. Strandberg, D. Suc and K. Wilson, *Science*, 1996, 271, 933.
- 140 G. Algara-Siller, N. Severin, S. Y. Chong, T. Björkman, R. G. Palgrave, A. Laybourn, M. Antonietti, Y. Z. Khimyak, A. V. Krasheninnikov and J. P. Rabe, *Angew. Chem.*, 2014, 126, 7580–7585.
- 141 K. Schwinghammer, M. B. Mesch, V. Duppel, C. Ziegler, J. Senker and B. V. Lotsch, *J. Am. Chem. Soc.*, 2014, 136, 1730–1733.
- 142 S. Samanta, S. Martha and K. Parida, *ChemCatChem*, 2014, 6, 1453–1462.
- 143 Y. Yang, Y. Guo, F. Liu, X. Yuan, Y. Guo, S. Zhang, W. Guo and M. Huo, *Appl. Catal.*, *B*, 2013, 142, 828–837.
- 144 Y. Bu, Z. Chen and W. Li, *Appl. Catal.*, *B*, 2014, 144, 622–630.
- 145 C. Chang, Y. Fu, M. Hu, C. Wang, G. Shan and L. Zhu, *Appl. Catal.*, *B*, 2013, 142, 553-560.
- 146 S. Bai, X. Wang, C. Hu, M. Xie, J. Jiang and Y. Xiong, Chem. Commun., 2014, 50, 6094–6097.
- 147 J. Yu, S. Wang, J. Low and W. Xiao, *Phys. Chem. Chem. Phys.*, 2013, 15, 16883–16890.
- 148 F. Raziq, Y. Qu, X. Zhang, M. Humayun, J. Wu, A. Zada, H. Yu, X. Sun and L. Jing, J. Phys. Chem. C, 2015, 120, 98–107.
- 149 G. Li, X. Nie, J. Chen, Q. Jiang, T. An, P. K. Wong, H. Zhang, H. Zhao and H. Yamashita, *Water Res.*, 2015, 86, 17–24.
- 150 Y. He, Y. Wang, L. Zhang, B. Teng and M. Fan, Appl. Catal., B, 2015, 168–169, 1–8.
- 151 C. Li, S. Wang, T. Wang, Y. Wei, P. Zhang and J. Gong, *Small*, 2014, **10**, 2783–2790.
- 152 T. Y. Ma, S. Dai, M. Jaroniec and S. Z. Qiao, *Angew. Chem.*, *Int. Ed.*, 2014, 53, 7281–7285.
- 153 G. Liao, S. Chen, X. Quan, H. Yu and H. Zhao, *J. Mater. Chem.*, 2012, 22, 2721–2726.
- 154 Z. Tong, D. Yang, J. Shi, Y. Nan, Y. Sun and Z. Jiang, ACS Appl. Mater. Interfaces, 2015, 7, 25693–25701.
- 155 X. Xia, N. Deng, G. Cui, J. Xie, X. Shi, Y. Zhao, Q. Wang, W. Wang and B. Tang, *Chem. Commun.*, 2015, 51, 10899–10902.
- 156 H. Zhang, L. Zhao, F. Geng, L. Guo, B. Wan and Y. Yang, Appl. Catal., B, 2016, 180, 656-662.
- 157 J. Liu, Y. Liu, N. Liu, Y. Han, X. Zhang, H. Huang, Y. Lifshitz, S. Lee, J. Zhong and Z. Kang, *Science*, 2015, 347, 970–974.
- 158 D. J. Martin, K. Qiu, S. A. Shevlin, A. D. Handoko, X. Chen, Z. Guo and J. Tang, *Angew. Chem., Int. Ed.*, 2014, 53, 9240–9245.
- 159 Y. Chen, B. Wang, S. Lin, Y. Zhang and X. Wang, *J. Phys. Chem. C*, 2014, **118**, 29981–29989.
- 160 Z. Huang, J. Song, L. Pan, Z. Wang, X. Zhang, J. Zou, W. Mi, X. Zhang and L. Wang, *Nano Energy*, 2015, 12, 646–656.

- 161 J. Zhang, M. Zhang, S. Lin, X. Fu and X. Wang, J. Catal., 2014, 310, 24–30.
- 162 L. Sun, Y. Qi, C. Jia, Z. Jin and W. Fan, *Nanoscale*, 2014, 6, 2649–2659.
- 163 J. Liu, J. Phys. Chem. C, 2015, 119, 28417-28423.
- 164 J. Wang, Z. Guan, J. Huang, Q. Li and J. Yang, J. Mater. Chem. A, 2014, 2, 7960–7966.
- 165 G. Gao, Y. Jiao, F. Ma, Y. Jiao, E. Waclawik and A. Du, *Phys. Chem. Chem. Phys.*, 2015, 17, 31140–31144.
- 166 J. Wirth, R. Neumann, M. Antonietti and P. Saalfrank, Phys. Chem. Chem. Phys., 2014, 16, 15917–15926.
- 167 X. Chen, S. Jia, N. Ding, J. Shi and Z. Wang, *Environ. Sci.: Nano*, 2016, 3, 1493–1503.
- 168 K. Li, S. Gao, Q. Wang, H. Xu, Z. Wang, B. Huang, Y. Dai and J. Lu, *ACS Appl. Mater. Interfaces*, 2015, 7, 9023–9030.
- 169 A. Mills and S. Le Hunte, *J. Photochem. Photobiol.*, A., 1997, 108, 1–35.
- 170 A. J. Frierdich, J. R. Shapley and T. J. Strathmann, *Environ. Sci. Technol.*, 2008, 42, 262–269.
- 171 T. Ye, D. P. Durkin, M. Hu, X. Wang, N. A. Banek, M. J. Wagner and D. Shuai, *ACS Appl. Mater. Interfaces*, 2016, 8, 17739–17744.
- 172 X. Feng, S. Zhu and H. Hou, Environ. Technol., 2006, 27, 119–126.
- 173 X. Zhang, T. Peng, L. Yu, R. Li, Q. Li and Z. Li, *ACS Catal.*, 2014, 5, 504–510.
- 174 R. A. Senthil, J. Theerthagiri, J. Madhavan, K. Murugan, P. Arunachalam and A. K. Arof, *J. Solid State Chem.*, 2016, 242, 199–206.
- 175 M. Grtzel, Acc. Chem. Res., 2009, 42, 1788-1798.
- 176 J. Ryu and W. Choi, *Environ. Sci. Technol.*, 2007, 42, 294–300.
- 177 Y. Nosaka, S. Komori, K. Yawata, T. Hirakawa and A. Y. Nosaka, *Phys. Chem. Chem. Phys.*, 2003, 5, 4731–4735.
- 178 K. McNeill and S. Canonica, *Environ. Sci.: Processes Impacts*, 2016, 18, 1381–1399.
- 179 C. M. Sharpless and N. V. Blough, Environ. Sci.: Processes Impacts, 2014, 16, 654-671.
- 180 T. Zeng and W. A. Arnold, Environ. Sci. Technol., 2012, 47, 6735-6745.
- 181 J. E. Grebel, J. J. Pignatello and W. A. Mitch, *Water Res.*, 2011, 45, 6535–6544.
- 182 F. L. Rosario-Ortiz and S. Canonica, *Environ. Sci. Technol.*, 2016, 50, 12532–12547.
- 183 S. Kohri, H. Fujii, S. Oowada, N. Endoh, Y. Sueishi, M. Kusakabe, M. Shimmei and Y. Kotake, *Anal. Biochem.*, 2009, 386, 167–171.
- 184 M. Kita and K. Ohara, J. Clin. Biochem. Nutr., 2014, 54, 67-74.
- 185 S. Qu, E. P. Kolodziej and D. M. Cwiertny, *Environ. Sci. Technol.*, 2012, **46**, 13202–13211.
- 186 J. M. Burns, W. J. Cooper, J. L. Ferry, D. W. King, B. P. DiMento, K. McNeill, C. J. Miller, W. L. Miller, B. M. Peake and S. A. Rusak, *Aquat. Sci.*, 2012, 74, 683–734.
- 187 E. Dez-Mato, F. C. Cortezn-Tamarit, S. Bogialli, D. Garca-Fresnadillo and M. D. Marazuela, *Appl. Catal.*, *B*, 2014, **160**, 445–455.

- 188 Y. Jing and B. P. Chaplin, *Environ. Sci. Technol.*, 2017, 51, 2355-2365
- 189 Y. Zhang, N. Zhang, Z. Tang and Y. Xu, Chem. Sci., 2013, 4, 1820–1824.
- 190 M. Hayyan, M. A. Hashim and I. M. AlNashef, *Chem. Rev.*, 2016, 116, 3029–3085.
- 191 M. Sun, Q. Yan, T. Yan, M. Li, D. Wei, Z. Wang, Q. Wei and B. Du, RSC Adv., 2014, 4, 31019–31027.
- 192 J. B. Sambur and P. Chen, J. Phys. Chem. C, 2016, 120, 20668–20676.
- 193 F. De Angelis, A. Tilocca and A. Selloni, *J. Am. Chem. Soc.*, 2004, 126, 15024–15025.
- 194 M. Pastore and F. De Angelis, *Phys. Chem. Chem. Phys.*, 2012, 14, 920-928.
- 195 J. Huang, W. Ho and X. Wang, *Chem. Commun.*, 2014, 50, 4338–4340.
- 196 W. Bing, Z. Chen, H. Sun, P. Shi, N. Gao, J. Ren and X. Qu, Nano Res., 2015, 8, 1648–1658.
- 197 S. Ma, S. Zhan, Y. Jia, Q. Shi and Q. Zhou, Appl. Catal., B, 2016, 186, 77–87.
- 198 Y. Li, C. Zhang, D. Shuai, S. Naraginti, D. Wang and W. Zhang, *Water Res.*, 2016, 106, 249–258.
- 199 W. Wang, J. C. Yu, D. Xia, P. K. Wong and Y. Li, Environ. Sci. Technol., 2013, 47, 8724–8732.
- 200 H. Zhao, H. Yu, X. Quan, S. Chen, Y. Zhang, H. Zhao and H. Wang, Appl. Catal., B, 2014, 152, 46–50.
- 201 A. S. Gong, C. A. Lanzl, D. M. Cwiertny and S. L. Walker, Environ. Sci. Technol., 2011, 46, 241–249.
- 202 G. Huang, D. Xia, T. An, T. W. Ng, H. Y. Yip, G. Li, H. Zhao and P. K. Wong, *Appl. Environ. Microbiol.*, 2015, 81, 5174–5183.
- 203 C. M. Hessler, M. Wu, Z. Xue, H. Choi and Y. Seo, Water Res., 2012, 46, 4687–4696.
- 204 Y. Liu, J. Li, X. Qiu and C. Burda, *J. Photochem. Photobiol.*, *A.*, 2007, **190**, 94–100.
- 205 S. Romero-Vargas Castrillón, F. Perreault, A. F. De Faria and M. Elimelech, *Environ. Sci. Technol. Lett.*, 2015, 2, 112–117.
- 206 S. Liu, T. H. Zeng, M. Hofmann, E. Burcombe, J. Wei, R. Jiang, J. Kong and Y. Chen, ACS Nano, 2011, 5, 6971–6980.
- 207 K. Rasool, M. Helal, A. Ali, C. E. Ren, Y. Gogotsi and K. A. Mahmoud, ACS Nano, 2016, 10, 3674–3684.
- 208 Y. Zhang, S. F. Ali, E. Dervishi, Y. Xu, Z. Li, D. Casciano and A. S. Biris, ACS Nano, 2010, 4, 3181–3186.
- 209 Y. Tu, M. Lv, P. Xiu, T. Huynh, M. Zhang, M. Castelli, Z. Liu, Q. Huang, C. Fan and H. Fang, Nat. Nanotechnol., 2013, 8, 594–601.
- 210 O. Akhavan and E. Ghaderi, ACS Nano, 2010, 4, 5731-5736.
- 211 T. Maisch, Photochem. Photobiol. Sci., 2015, 14, 1518-1526.
- 212 R. Leclercq and P. Courvalin, *Antimicrob. Agents Chemother.*, 1991, 35, 1267.
- 213 K. J. Flynn and M. S. Swanson, mBio, 2014, 5, 1091.
- 214 Q. Zhong, A. Carratalà, S. Nazarov, R. C. Guerrero-Ferreira, L. Piccinini, V. Bachmann, P. G. Leiman and T. Kohn, *Environ. Sci. Technol.*, 2016, 50, 13520–13528.
- 215 N. Czekalski, S. Imminger, E. Salhi, M. Veljkovic, K. Kleffel, D. Drissner, F. Hammes, H. Bürgmann and U. von Gunten, *Environ. Sci. Technol.*, 2016, 50, 11862–11871.

- 216 P. Dunlop, M. Ciavola, L. Rizzo, D. A. McDowell and J. A. Byrne, *Catal. Today*, 2015, 240, 55–60.
- 217 C. F. Jones and D. W. Grainger, Adv. Drug Delivery Rev., 2009, 61, 438–456.
- 218 D. K. Dennison and T. E. Dyke, *Periodontol. 2000*, 1997, 14, 54–78.
- 219 V. H. Grassian, *Nanoscience and nanotechnology:* environmental and health impacts, John Wiley & Sons, 2008.
- 220 K. L. Aillon, Y. Xie, N. El-Gendy, C. J. Berkland and M. L. Forrest, *Adv. Drug Delivery Rev.*, 2009, **61**, 457–466.
- 221 K. C. Christoforidis, M. Melchionna, T. Montini, D. Papoulis, E. Stathatos, S. Zafeiratos, E. Kordouli and P. Fornasiero, RSC Adv., 2016, 6, 86617–86626.
- 222 P. G. Tratnyek and J. Hoigne, *Environ. Sci. Technol.*, 1991, 25, 1596–1604.
- 223 S. C. Yan, Z. S. Li and Z. G. Zou, *Langmuir*, 2009, 25, 10397–10401.
- 224 X. Huang, M. Leal and Q. Li, Water Res., 2008, 42, 1142–1150.
- 225 J. Brame, M. Long, Q. Li and P. Alvarez, Water Res., 2014, 60, 259-266.
- 226 J. Brame, M. Long, Q. Li and P. Alvarez, Water Res., 2015, 84, 362-371.
- 227 S. Carbonaro, M. N. Sugihara and T. J. Strathmann, *Appl. Catal.*, *B*, 2013, 129, 1–12.
- 228 T. Ohno, L. Bai, T. Hisatomi, K. Maeda and K. Domen, I. Am. Chem. Soc., 2012, 134, 8254–8259.
- 229 E. L. Cates, Environ. Sci. Technol., 2017, 51, 757-758.
- 230 National Research Council, Safe water from every tap: improving water service to small communities, National Academies Press, 1997.
- 231 USEPA, Report: Much Effort and Resources Needed to Help Small Drinking Water Systems Overcome Challenges, 2006-P-00026, Office of Inspector General, U.S. Environmental Protection Agency, Washington, DC, 2006.
- 232 USEPA, Drinking Water and Ground Water Statistics, fiscal year 2011, HERO 2533123, Office of Water, U.S.

- Environmental Protection Agency, Washington, DC, 2013.
- 233 USEPA, *Drinking water: past, present, and future, EPA 816-F-00-002, Office of Water*, U.S. Environmental Protection Agency, Washington, DC, 2000.
- 234 R. J. Braham and A. T. Harris, *Ind. Eng. Chem. Res.*, 2009, 48, 8890–8905.
- 235 D. Spasiano, R. Marotta, S. Malato, P. Fernandez-Ibanez and I. Di Somma, *Appl. Catal.*, *B*, 2015, 170, 90–123.
- 236 V. Augugliaro, E. Garcia-Lopez, V. Loddo, S. Malato-Rodriguez, I. Maldonado, G. Marc, R. Molinari and L. Palmisano, *Sol. Energy*, 2005, 79, 402–408.
- 237 P. Fernndez, J. Blanco, C. Sichel and S. Malato, *Catal. Today*, 2005, **101**, 345–352.
- 238 P. Fernandez-Ibaez, S. Malato and O. Enea, *Catal. Today*, 1999, 54, 329–339.
- 239 P. Pichat, S. Vannier, J. Dussaud and J. Rubis, *Sol. Energy*, 2004, 77, 533–542.
- 240 C. Sichel, J. Tello, M. De Cara and P. Fernndez-Ibez, *Catal. Today*, 2007, 129, 152–160.
- 241 S. Malato, J. Blanco, C. Richter, D. Curco and J. Gimenez, Water Sci. Technol., 1997, 35, 157–164.
- 242 N. Miranda-Garca, S. Surez, B. Snchez, J. M. Coronado, S. Malato and M. I. Maldonado, Appl. Catal., B, 2011, 103, 294–301.
- 243 M. I. Polo-López, P. Fernández-Ibáñez, I. García-Fernández, I. Oller, I. Salgado-Tránsito and C. Sichel, J. Chem. Technol. Biotechnol., 2010, 85, 1038–1048.
- 244 J. Blanco, S. Malato, P. Fernndez, A. Vidal, A. Morales, P. Trincado, J. C. Oliveira, C. Minero, M. Musci and C. Casalle, Sol. Energy, 1999, 67, 317–330.
- 245 S. Malato, J. Blanco, A. Vidal, P. Fernndez, J. Cceres, P. Trincado, J. C. Oliveira and M. Vincent, *Chemosphere*, 2002, 47, 235–240.
- 246 C. Navntoft, P. Araujo, M. I. Litter, M. C. Apella, D. Fernndez, M. E. Puchulu, M. d. V. Hidalgo and M. A. Blesa, J. Sol. Energy Eng., 2007, 129, 127–134.